Dual Ion Conductivity in Hexagonal Perovskite Derivatives

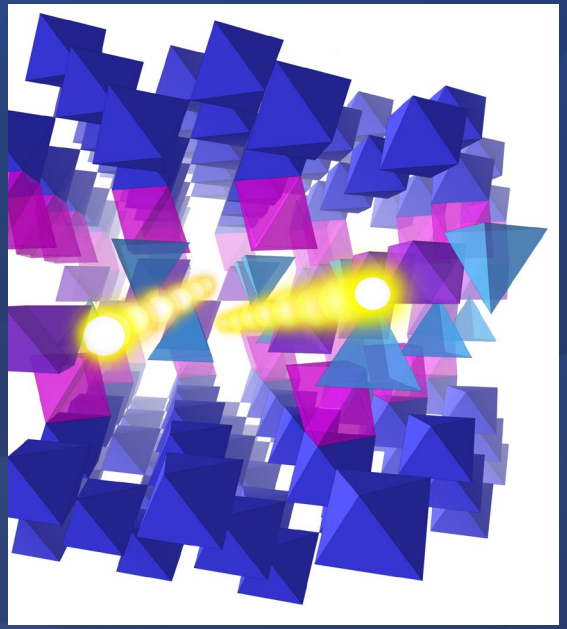

Abbie Mclaughlin
October 2023

1495 UNIVERSITY OF ABERDEEN

Introduction

The Structural and Electrical Properties of :

$Ba_3M'M''O_{8.5}$ phases (M' = Nb, V; M'' = Mo, W)

$Ba_7Nb_4MoO_{20}$ – a new oxide ion/proton conductor

Ionic conducting palmierites – $A_3V_2O_8$

Summary

Acknowledgements

Combat climate change – new materials and methods are needed.

To achieve net zero emissions by 2050, it is predicted that one third of the UK's energy consumption must be hydrogen-based.

Ceramic fuel cells – key role

Solid Oxide Fuel Cells

Generates energy by clean, efficient and environmental-friendly means.

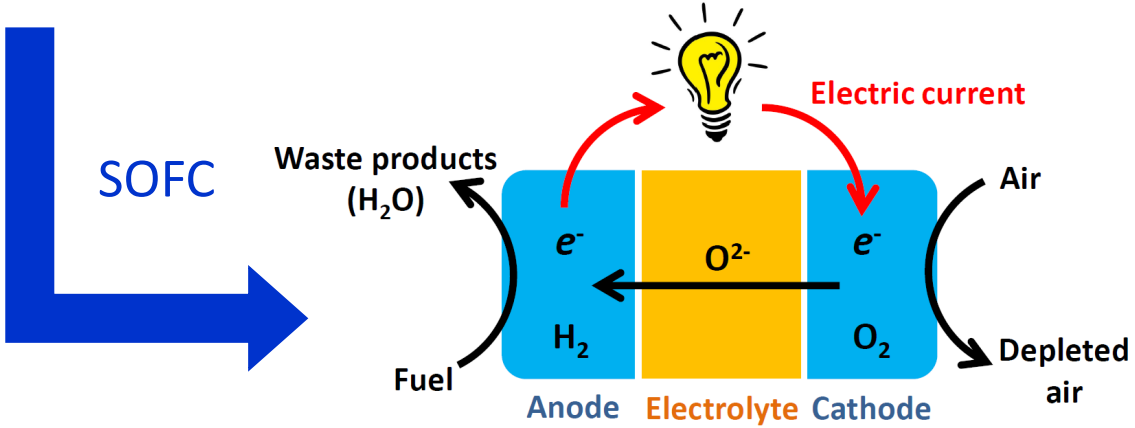

The electrolyte for a SOFC is a solid ceramic inorganic oxide that possesses high oxide ion conductivity and negligible electronic conductivity.

Electrolyte

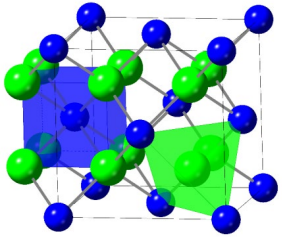

Fluorite AO_2
YSZ, GDC, δ-Bi_2O_3

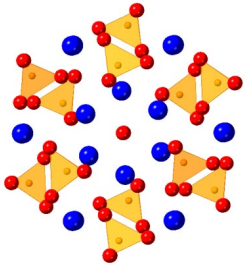

Apatites
$La_{10-x}(XO_4)_6O_{2\pm\delta}$
X = Si, Ge

Challenge in SOFC technology:
reducing the working temperature to < 600 °C
Discover new structural families of oxide ion conducting materials

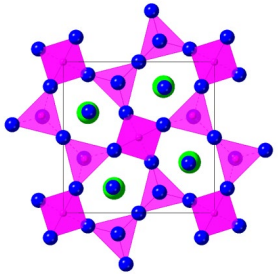

Melilite
$La_{1+x}Sr_{1-x}Ga_3O_{7-\delta}$

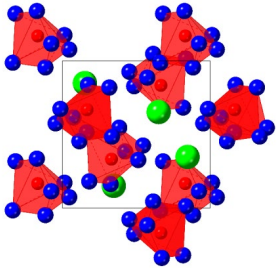

LAMOX
$La_2Mo_2O_9$

1495 UNIVERSITY OF ABERDEEN

Proton Ceramic Fuel Cells

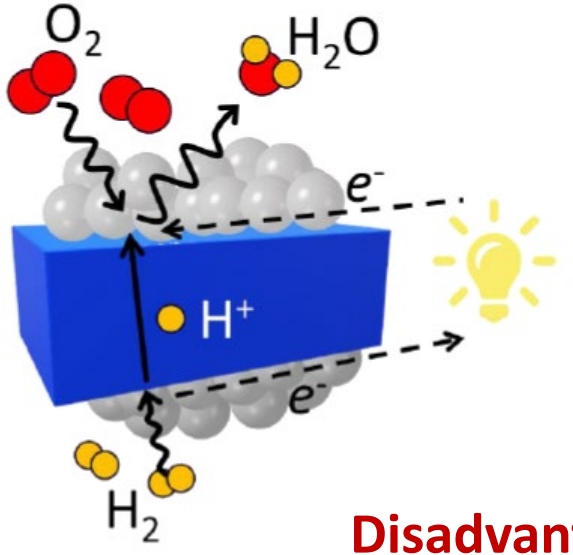

Uses a solid electrolyte which is a proton conductor.

Advantages: High ionic conductivity can be observed at 400 – 500 °C.

Disadvantages: The best materials so far are reactive with CO_2 or require expensive processing.

Perovskite family

Perfect structure to discover new oxide ion and proton conductors due to its capability of adopting numerous structural derivatives.

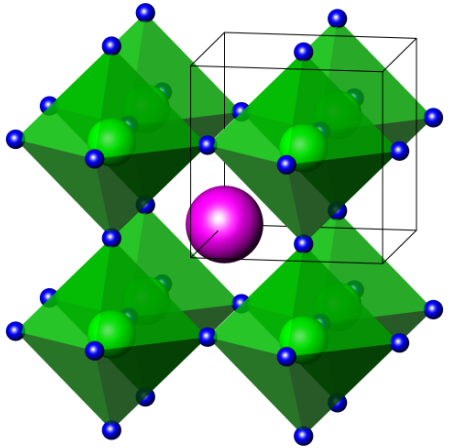

Oxide ion conductors:
Sr doped $LaGaO_3$ and
$Na_{0.5}Bi_{0.5}TiO_3$

T. Ishihara *et al. J. Am. Chem. Soc.* 116, 3801–3803 (1994).
M. Li *et al. Nat. Mater.* 13, 31–5 (2014).

Perovskite family

Perfect structure to discover new oxide ion and proton conductors due to its capability of adopting numerous structural derivatives.

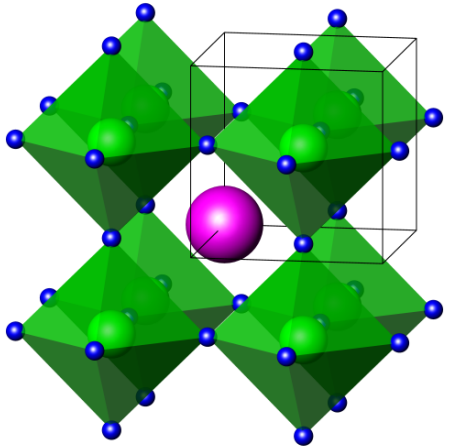

Proton conductors:
$BaCe_{1-x}Y_xO_{3-\delta}$ and
$BaZr_{1-x}Y_xO_{3-\delta}$

T. Ishihara *et al. J. Am. Chem. Soc.* 116, 3801–3803 (1994).
M. Li *et al. Nat. Mater.* 13, 31–5 (2014).

Hexagonal perovskites

Mixed stacking combinations lead to an infinite number of hexagonal polytypic derivatives

Potential to possess structural features able to support oxide ion and proton conduction

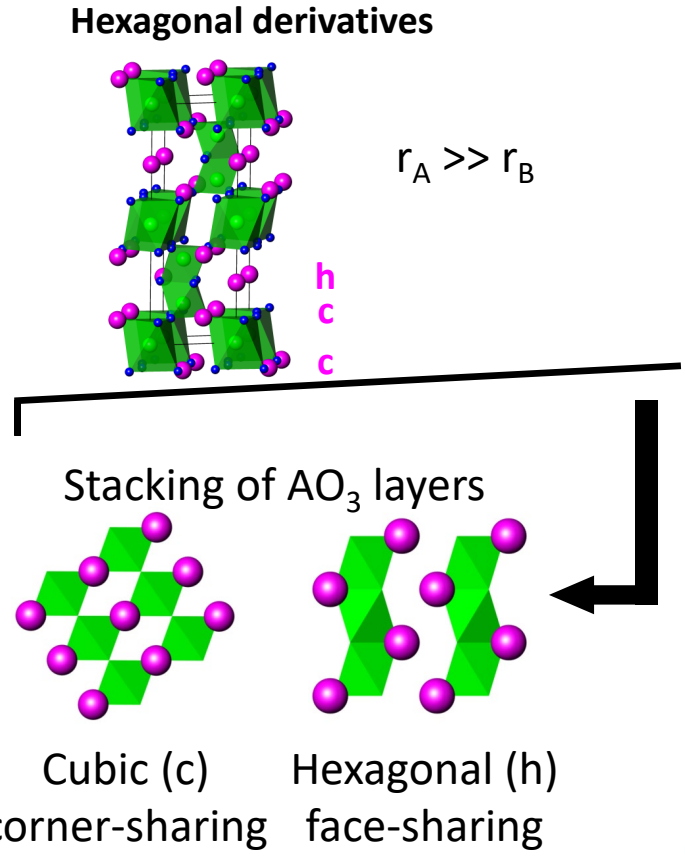

Hexagonal perovskites

Mixed oxide/proton/electronic conductivity has been observed in $Ba_4M_2O_9$ (M = Nb, Ta, Sb).

Multiple polymorphs

Ionic contribution is < 25 % for $Ba_4Ta_2O_9$ and $Ba_4Nb_2O_9$.

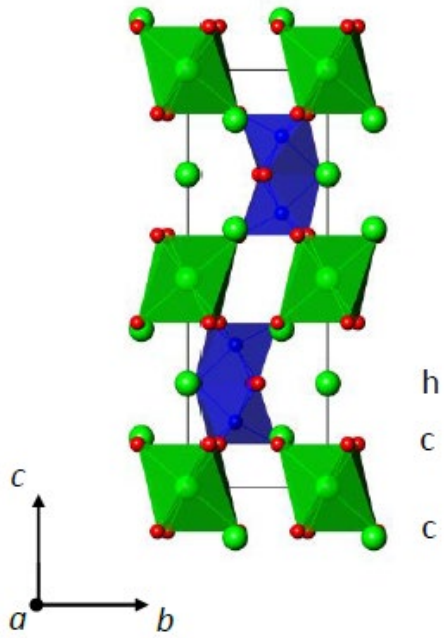

C. Ling *et al. Chem. Mater.* 21, 3853 (2009).
C. Ling *et al. Chem. Mater. 22*, 532 (2009).

Hexagonal perovskites

Titanates such as $Ba_6Y_2Ti_4O_{17}$ and $Ba_7Y_2Mn_3Ti_2O_{20}$.

Mixed ionic and electronic conduction.

Ionic component ~ 35 %.

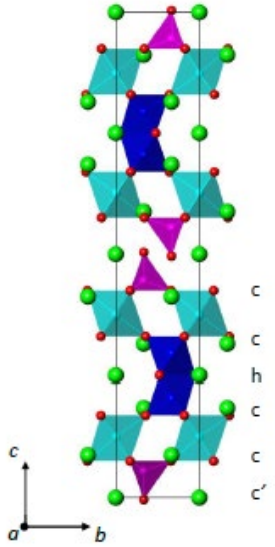

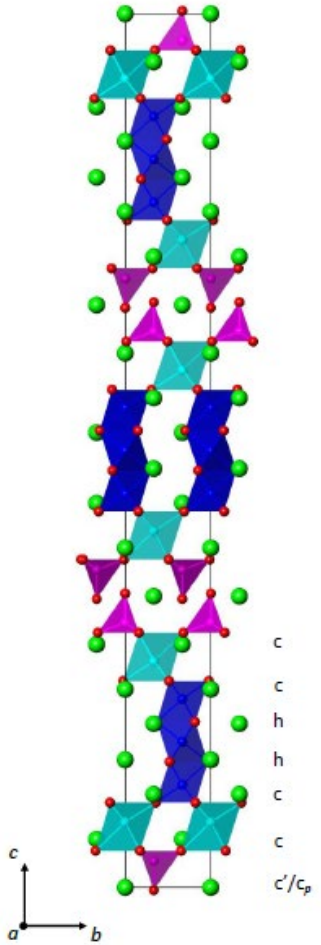

X. Kuang *et al. Chem. Mater.* 14, 4359 (2002).
X. Kuang *et al. Chem. Mater. 19*, 2884 (2007).

The Structural and Electrical Properties of $Ba_3M'M''O_{8.5}$ phases

(M’ = Nb, V; M’’ = Mo, W)

1495 UNIVERSITY OF ABERDEEN

$Ba_3NbMoO_{8.5}$ is the first hexagonal perovskite derivative to exhibit significant oxide ion conductivity.

Bulk conductivity comparable to other leading solid oxide conductors

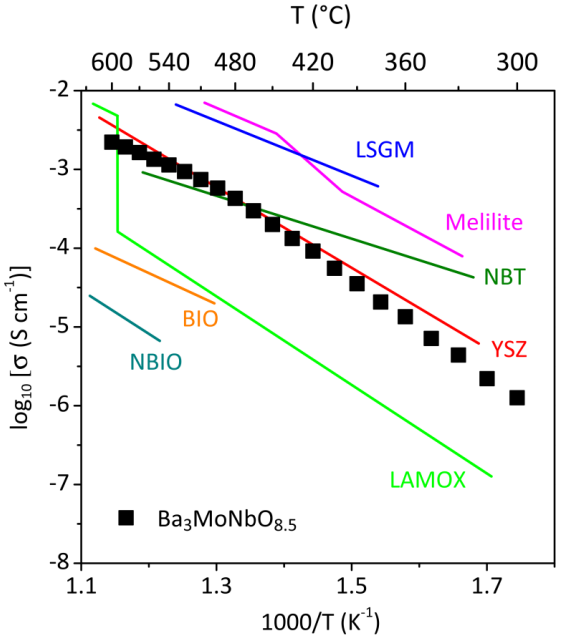

$Zr_{0.92}Y_{0.08}O_{1.96}$ (YSZ), $La_{0.9}Sr_{0.1}Ga_{0.8}Mg_{0.2}O_3$ (LSGM), $La_2Mo_2O_9$ (LAMOX), $Na_{0.5}Bi_{0.5}TiO_3$ (NBT), $La_{1.54}Sr_{0.46}Ga_3O_{7.27}$ (Melilite), $Ba_2In_2O_5$ (BIO) and $NdBaInO_4$ (NBIO)

S. Fop *et al. JACS* 138, 16764 (2016).

$Ba_3NbMoO_{8.5}$ is the first hexagonal perovskite derivative to exhibit significant oxide ion conductivity.

Ionic contribution > 99% in air/O_2 – negligible electronic component

Ionic contribution > 94% in air/5% H_2 in Ar - a small amount of electronic conduction is observed

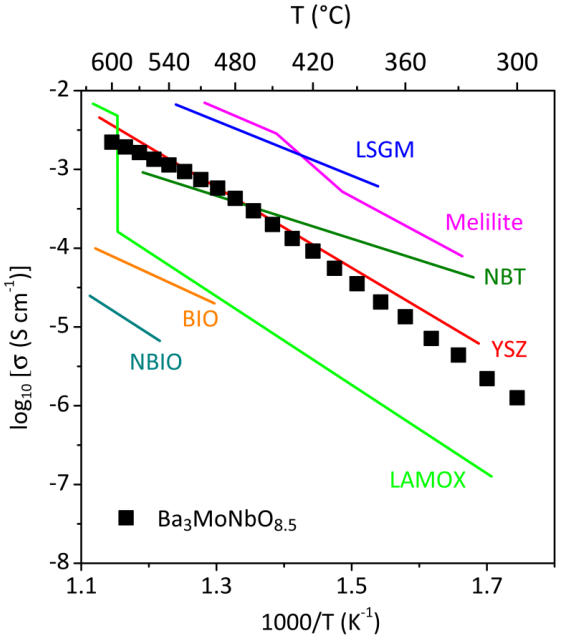

$Zr_{0.92}Y_{0.08}O_{1.96}$ (YSZ), $La_{0.9}Sr_{0.1}Ga_{0.8}Mg_{0.2}O_3$ (LSGM), $La_2Mo_2O_9$ (LAMOX), $Na_{0.5}Bi_{0.5}TiO_3$ (NBT), $La_{1.54}Sr_{0.46}Ga_3O_{7.27}$ (Melilite), $Ba_2In_2O_5$ (BIO) and $NdBaInO_4$ (NBIO)

S. Fop *et al. JACS* 138, 16764 (2016).

Structural Model (neutron diffraction (GEM))

Hybrid model formed by the superimposition of two structural sub-units.

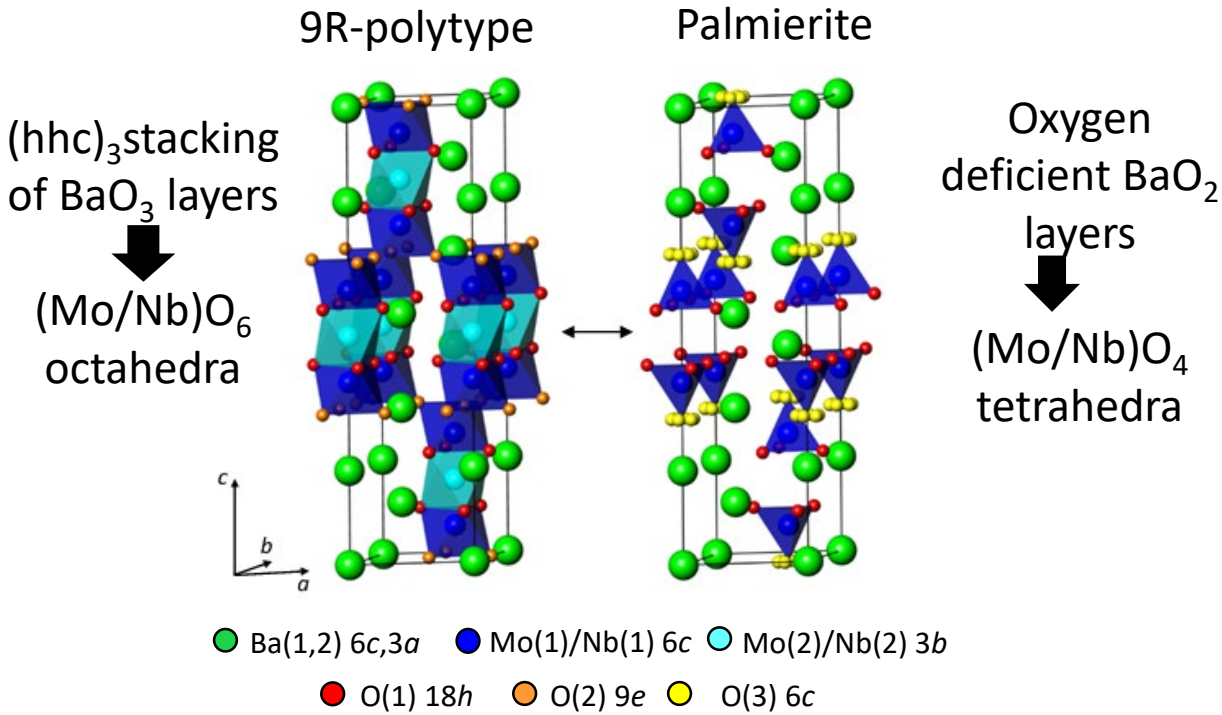

UNIVERSITY OF ABERDEEN

Structural Model (neutron diffraction (GEM))

Disordered distribution of Mo/Nb tetrahedra and octahedra

Intrinsic oxygen vacancies

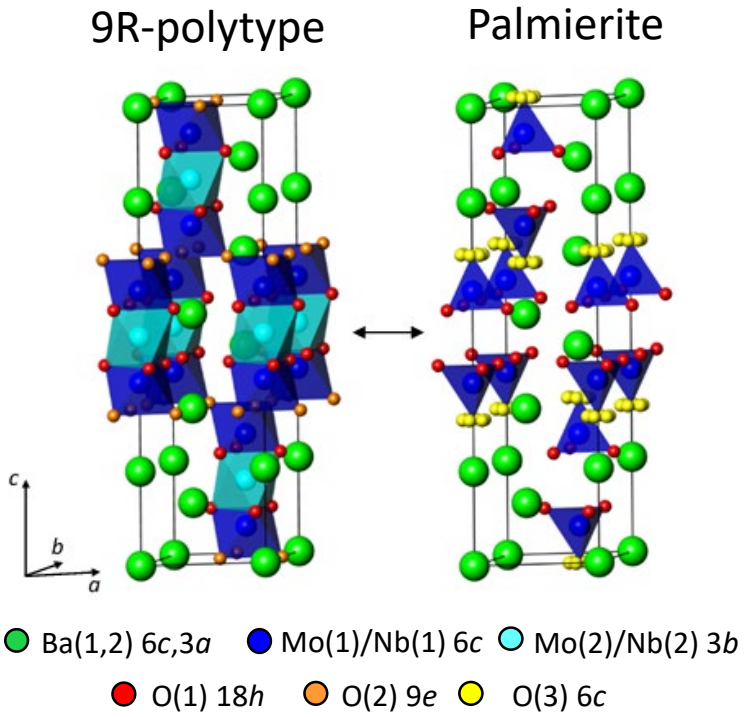

Variable Temperature Neutron Diffraction Study (D2B, ILL)

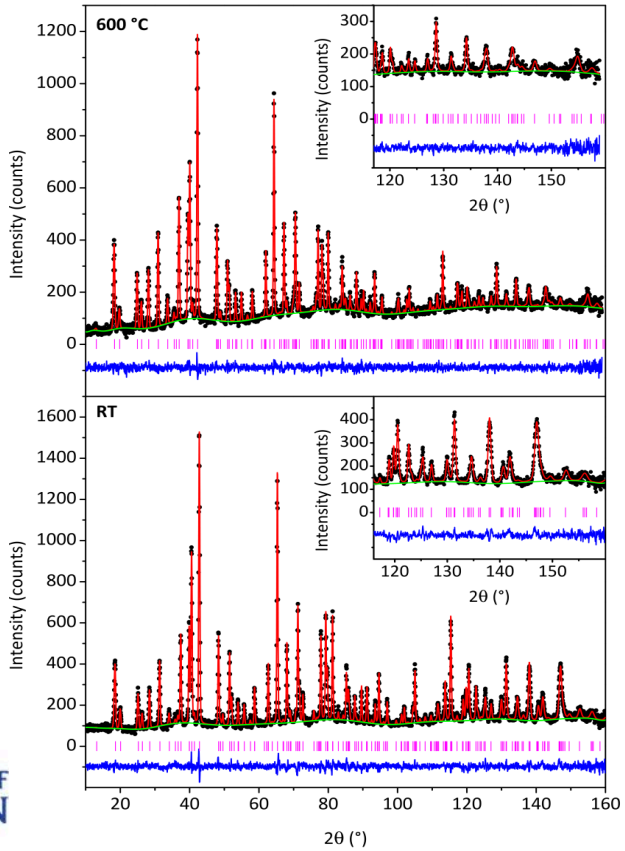

No change in crystal symmetry upon heating to 600 °C.

Excellent fit to the *R*-3*m* H hybrid model at both temperatures.

UNIVERSITY OF ABERDEEN

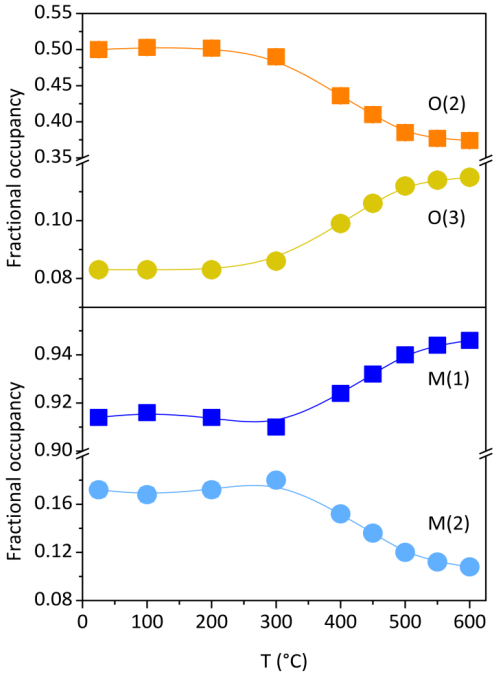

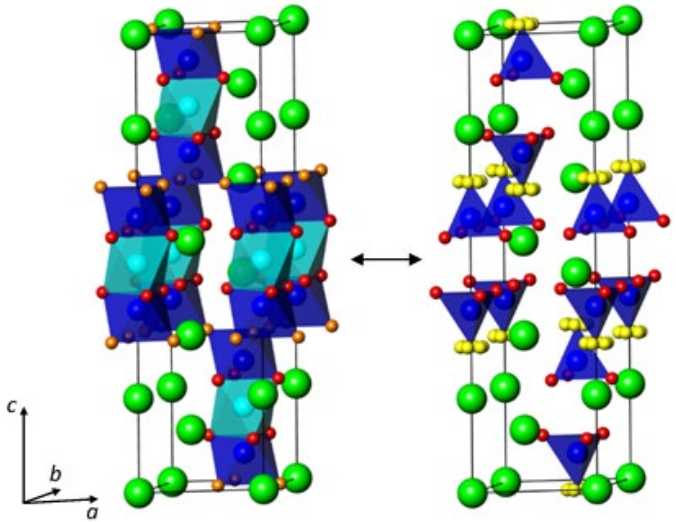

Increase in number of (Mo/Nb)O_4 tetrahedra.

The structure is able to adjust the ratio of tetraheda to octahedra and, consequently, oxygen/vacancy distributions as the temperature increases.

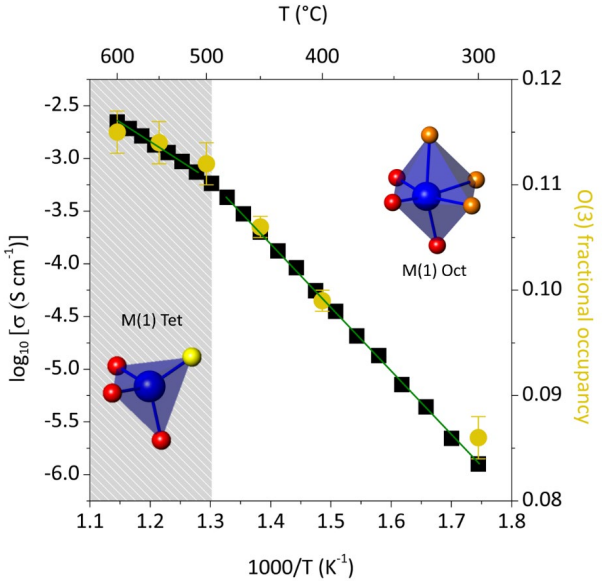

There is a strong correlation between the bulk conductivity and the structural rearrangement.

At 300 °C there are ~ 50% tetrahedra within the average structure which increases to 65% at 600 °C.

Increase the number of tetrahedra by selected chemical substitution to tune the conductivity?

UNIVERSITY OF ABERDEEN

S. Fop *et al Chem. Mater.* 29, 4146 (2017).

$Ba_3Nb_{1-x}V_xMoO_{8.5}$ has been synthesised.

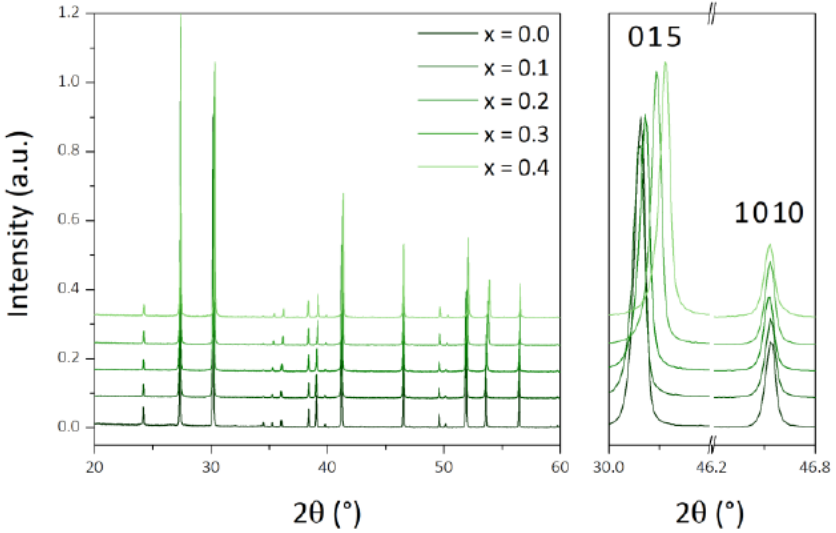

Samples are phase pure and stable upon heating in air, O_2, N_2 or 5% H_2/N_2 for 48 hours.

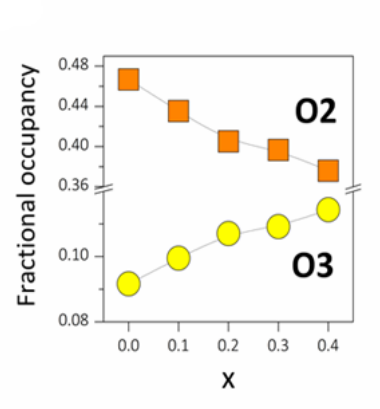

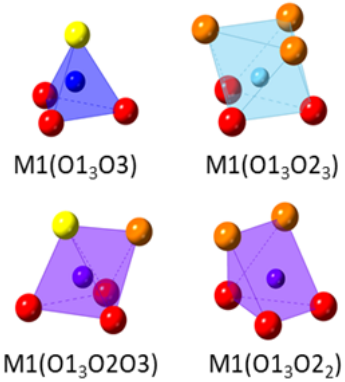

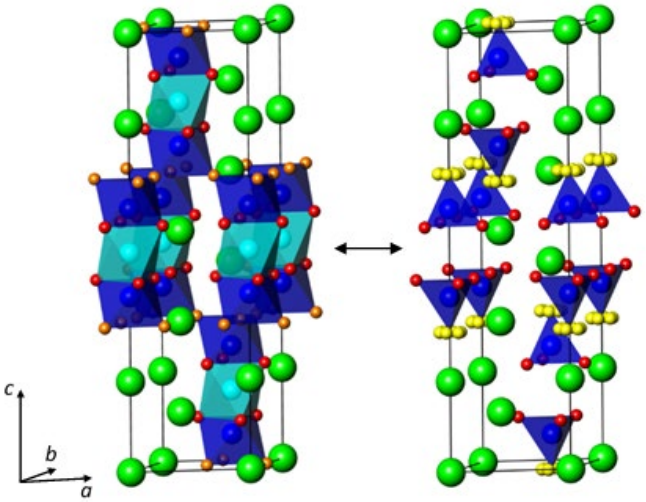

Rietveld refinement of the structural model from both neutron and high-resolution laboratory X-ray diffraction data.

UNIVERSITY OF ABERDEEN

S. Fop et al, *Chem. Mater.*, 2020, 32, 4724.

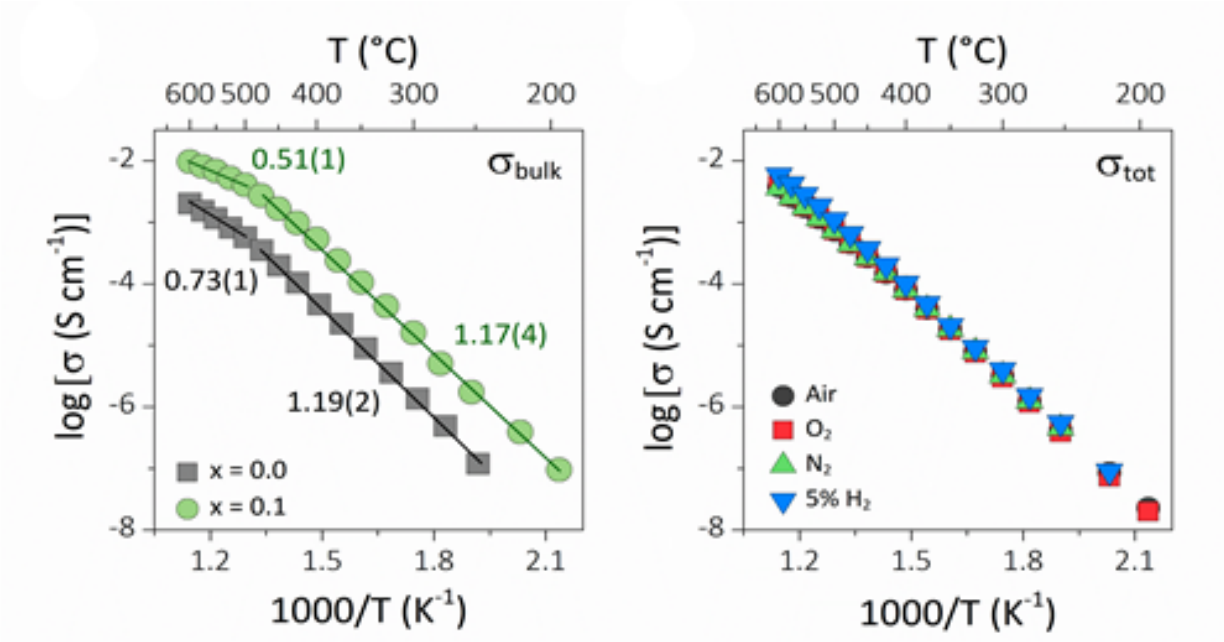

The bulk conductivity of $Ba_3Nb_{0.9}V_{0.1}MoO_{8.5}$ is almost an order of magnitude higher than that of $Ba_3NbMoO_{8.5}$.

UNIVERSITY OF ABERDEEN

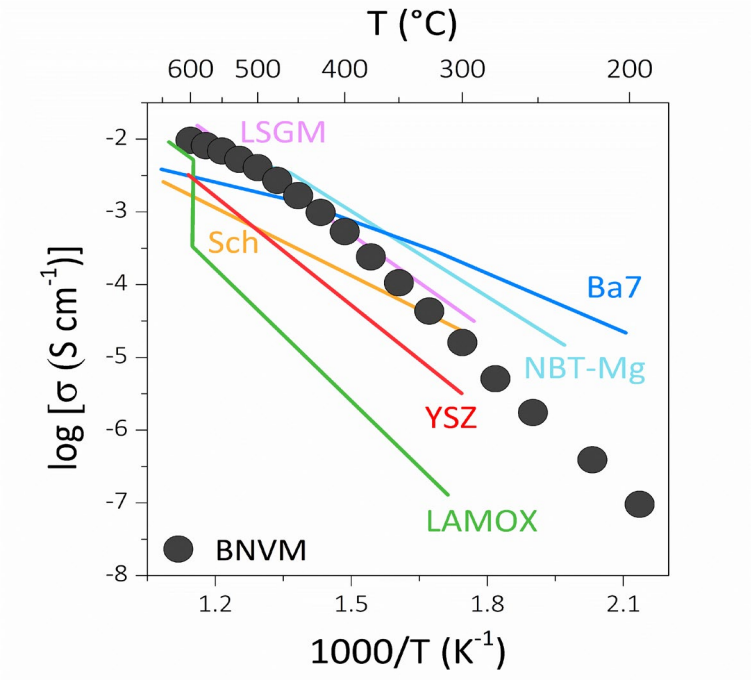

The bulk conductivity of is as good as the best materials reported.

S. Fop et al, *Chem. Mater.*, 2020, 32, 4724.

Bond-valence site energy calculations using *soft*BV.
Map out migration pathway and energy landscape.

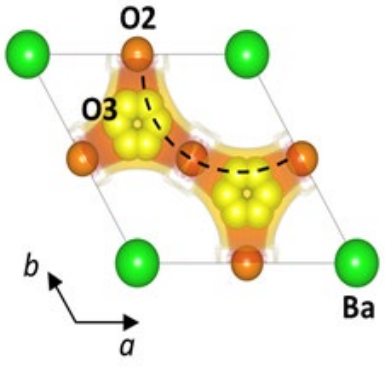

Predominant pathway is two-dimensional with oxide ion diffusion through the partially occupied O2 and O3 oxygen sites.

UNIVERSITY OF ABERDEEN

H. Chen *et al*. *Acta Crystallographica Section B* 75, 18-33 (2019).

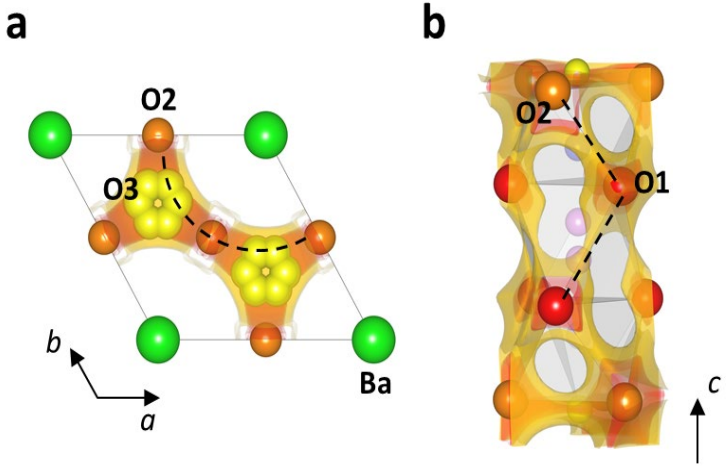

Also oxide ion motion between O(1) and O(2) and O(1) and O(1) along the edges of the $M1O_x$ and $M2O1_6$ polyhedral. Much larger bond valence activation barrier (> 1.1 eV)

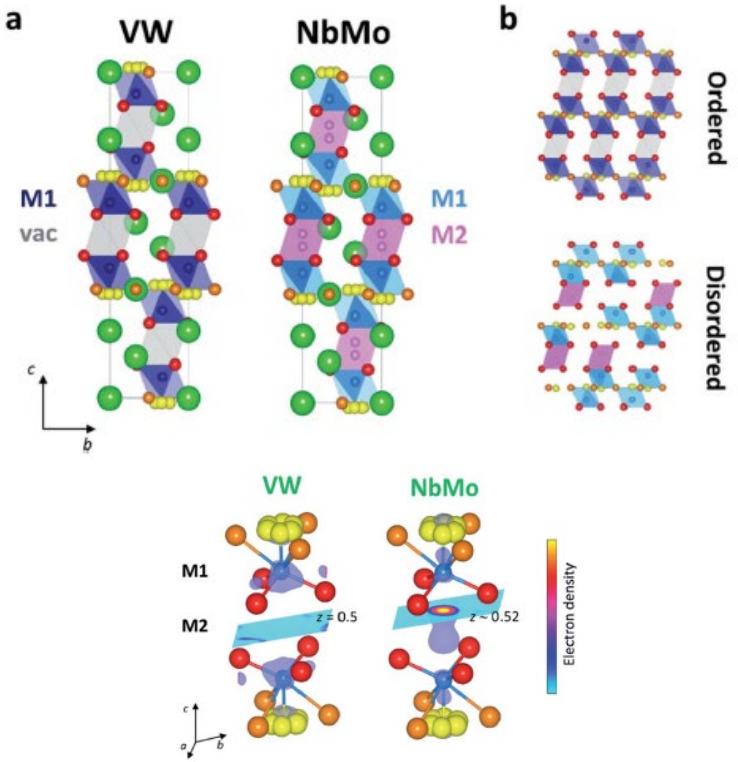

$Ba_3VWO_{8.5}$ and $Ba_3VMoO_{8.5}$ have now been synthesised.

Cation vacancies are ordered.

A. Gilane *et al*, *J. Mat. Chem. A*, **8**, 16506 – 16514 (2020).

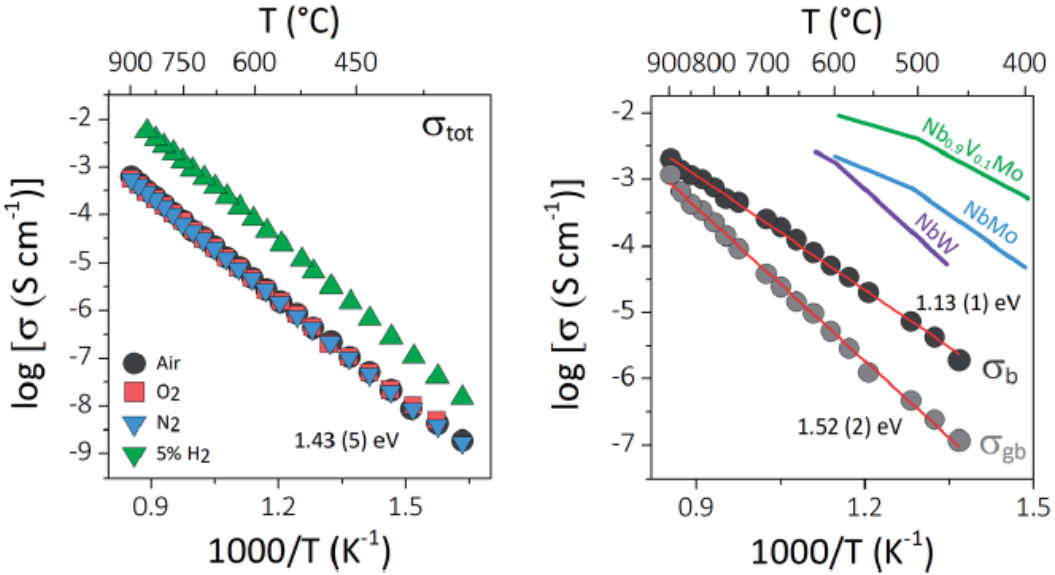

$Ba_3VWO_{8.5}$ is an oxide ion conductor, although the conductivity is lower than the Nb materials.

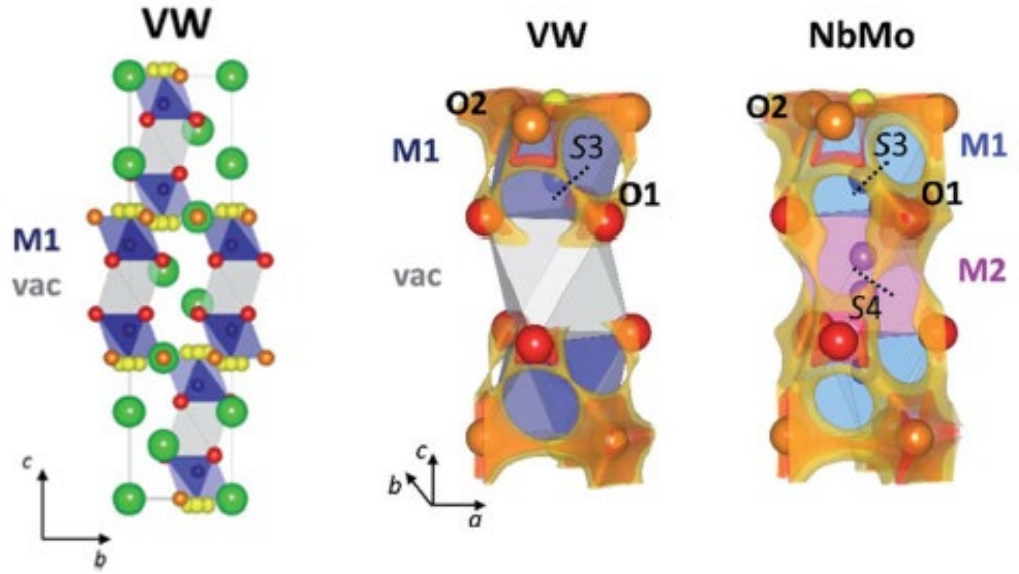

BVSE analysis shows no 3D connectivity in $Ba_3VWO_{8.5}$.

Ordering of the cation vacancies disrupts the conductivity along *c* and leads to reduced conductivity compared to other $Ba_3M'M''O_{8.5}$ phases.

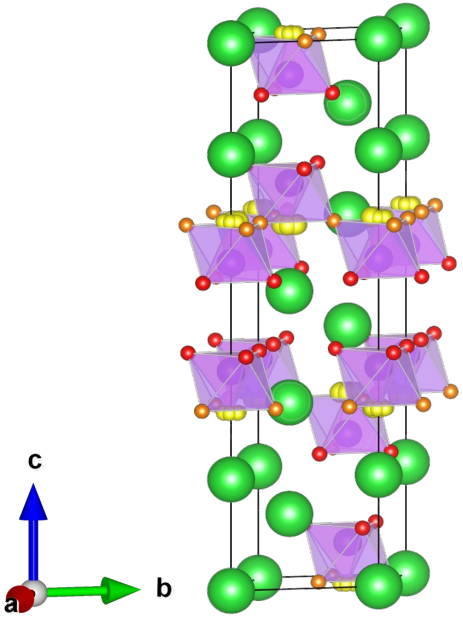

$Ba_3VMoO_{8.5}$ has Ba and oxygen vacancies: $Ba_{2.69}VMoO_{8.20}$

Unstable above 300°C.

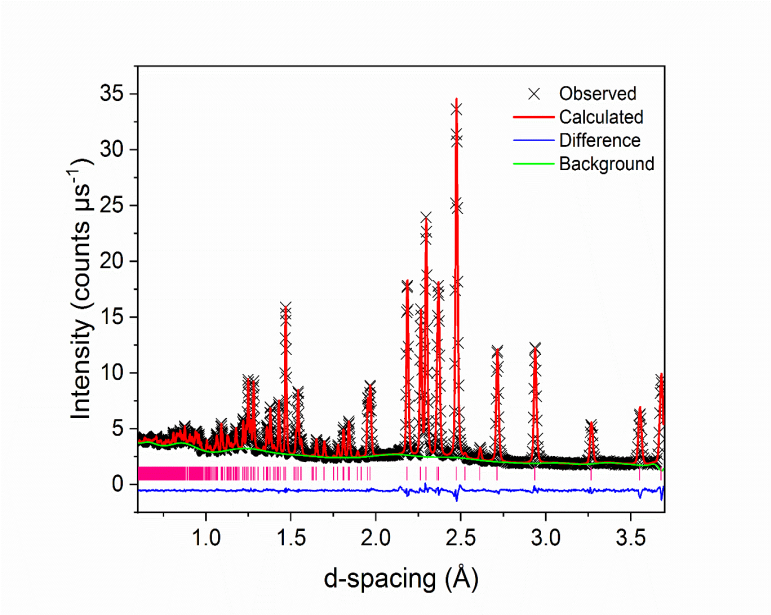

1495 UNIVERSITY OF ABERDEEN

$Ba_7Nb_4MoO_{20}$ – a new oxide ion/proton conductor

$Ba_7Nb_4MoO_{20}$ – a new oxide ion/proton conductor

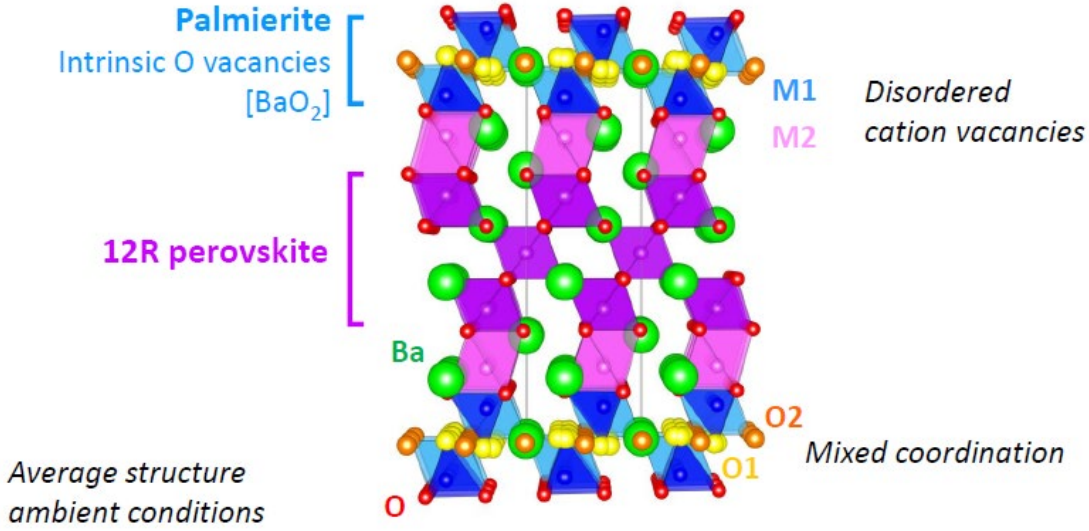

Neutron diffraction on the D2B instrument, ILL shows that at room temperature the crystal structure is very disordered.

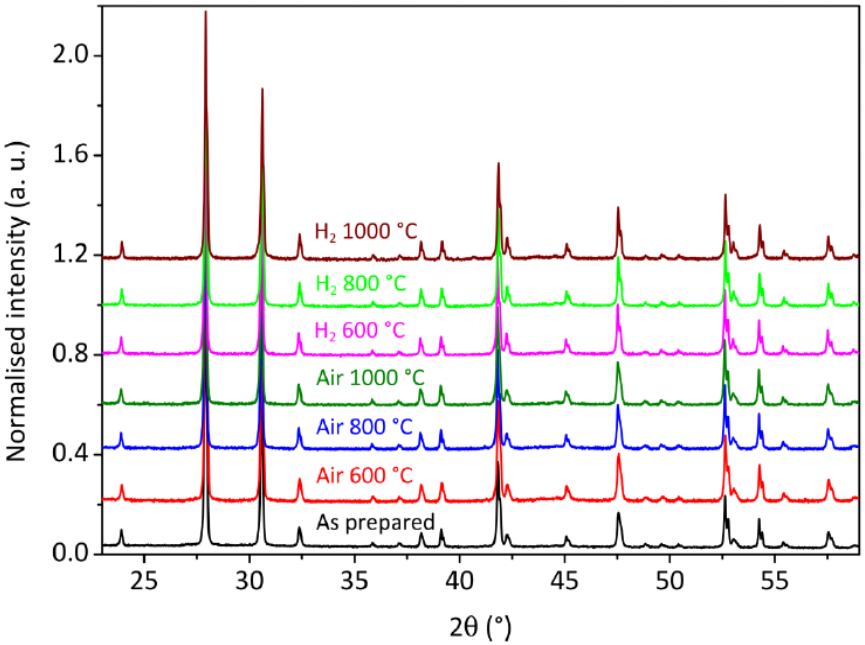

$Ba_7Nb_4MoO_{20}$ is stable after being annealed in a range of oxidising and reducing gases.

Electrical Measurements – dry air

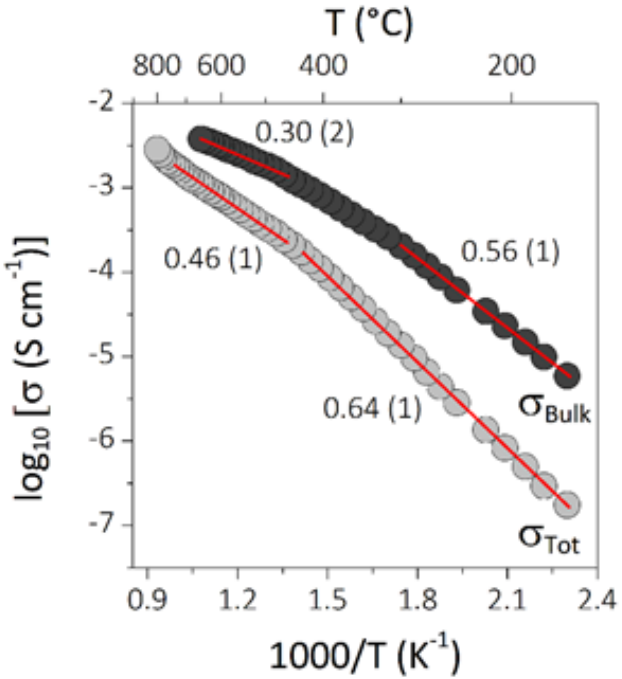

Transport measurements show negligible electronic conductivity in air/O_2 or air/5% H_2 in Ar.

The ionic contribution is > 99%.

Electrical Measurements – wet air

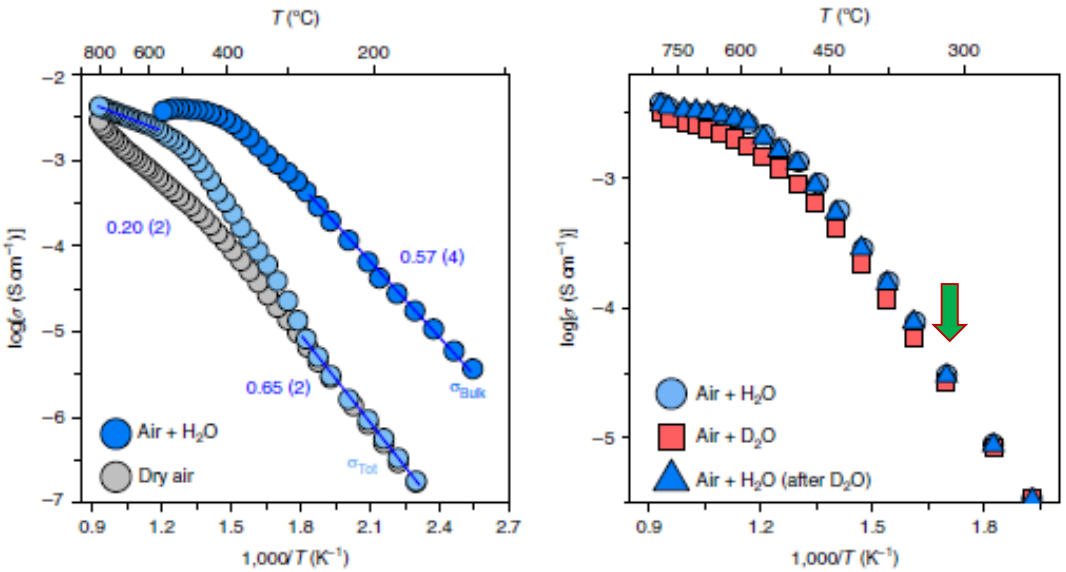

Above 300 °C the conductivity increases in humidified air suggesting proton conduction.

Clear isotope effect.

S. Fop et al, *Nature Mater.*, 2020, 19, 752.

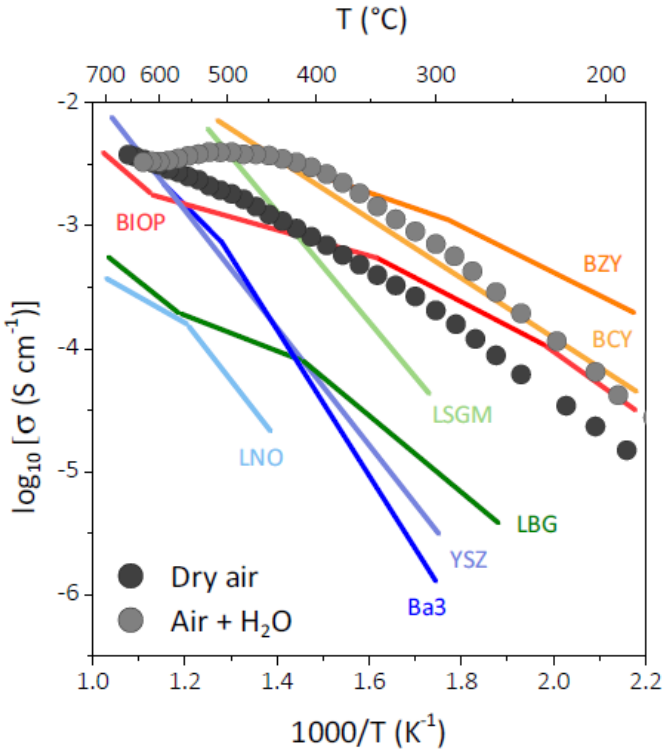

Significant proton conductivity comparable to leading solid proton conductors. σ = 4 mS cm^{-1} at 500 °C

The phase is stable in CO_2 up to 700 °C.

S. Fop *et al*, *Nature Mater.*, 2020, 19, 752.

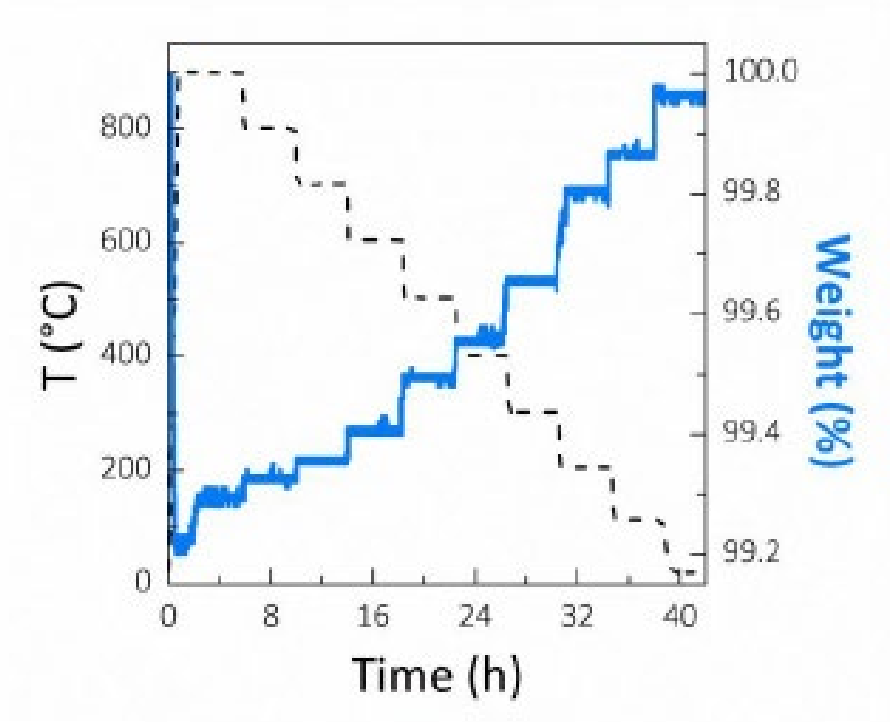

Uniform water uptake

$Ba_7Nb_4MoO_{20} \cdot 0.8H_2O$

In-situ neutron diffraction - HRPD

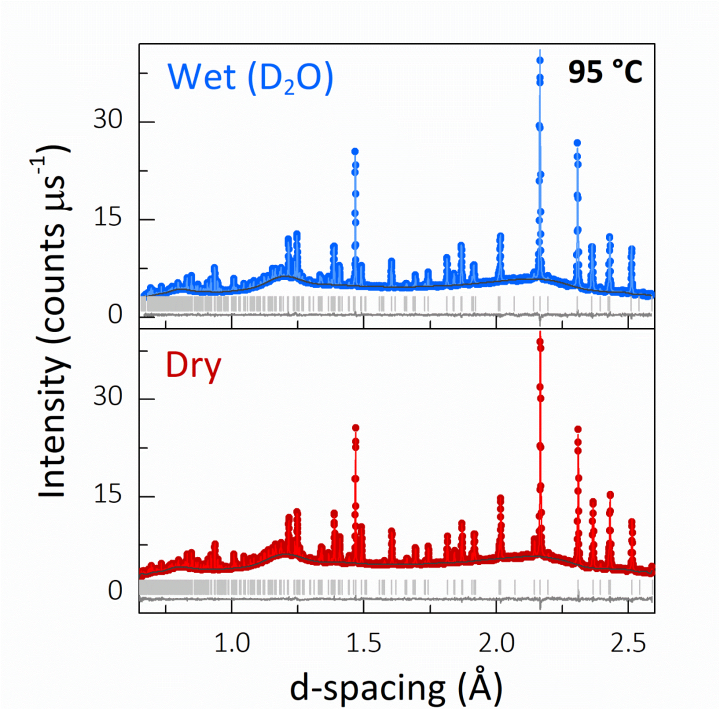

Under dry and humidified conditions.
Excellent fit to the $P\bar{3}m1$ space group. No change in the space group with temperature.

UNIVERSITY OF ABERDEEN

Dry Conditions

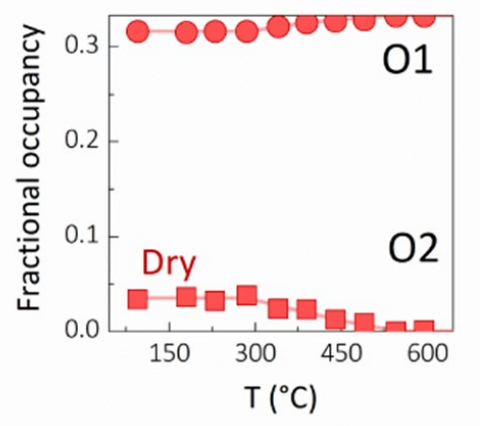

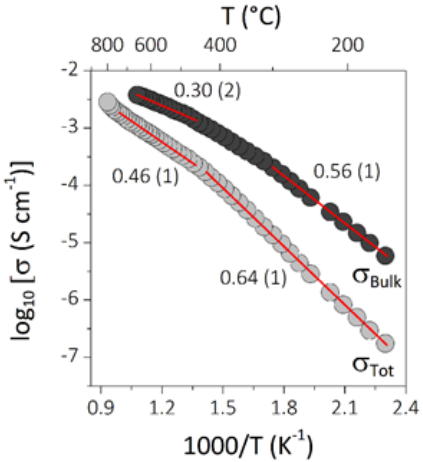

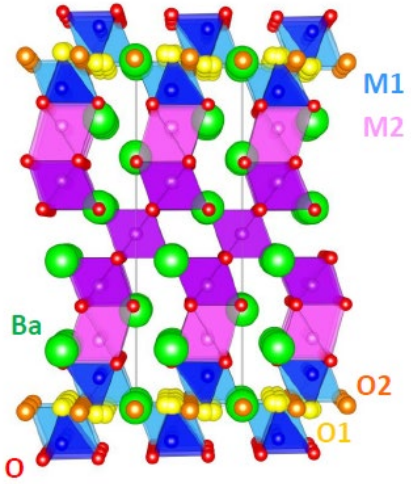

In dry conditions O1 is predominantly occupied.

Structural re-organisation above 300 °C.

Wet Conditions

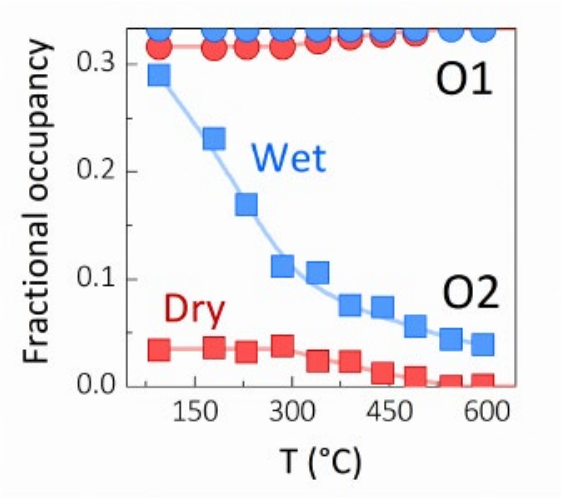

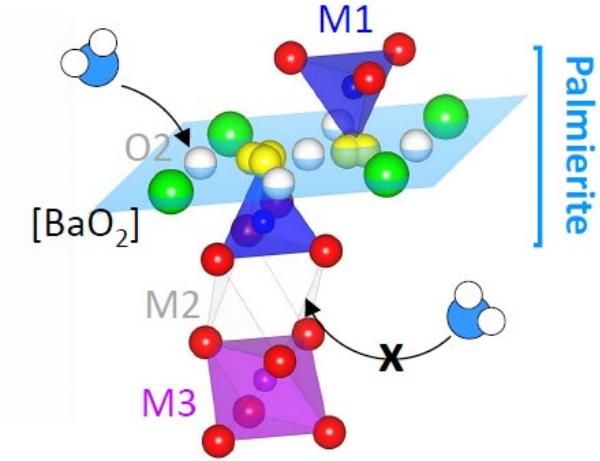

Water is predominantly entering at the vacant O2 site.

Rapid increase in H_2O uptake below 300 °C.

S. Fop *et al*, *Chem. Mater.* 33, 4651 (2021).

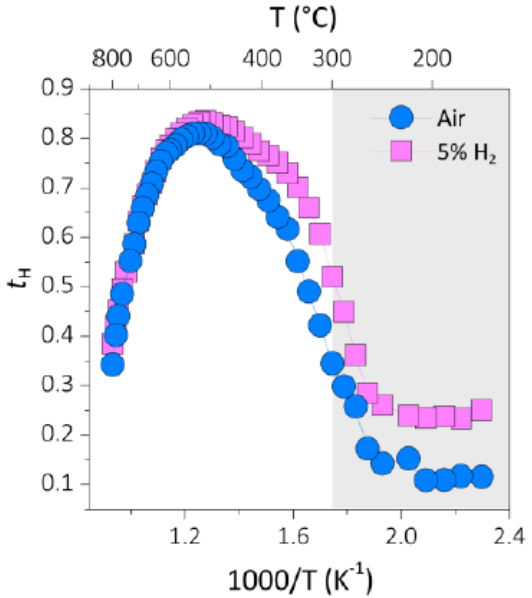

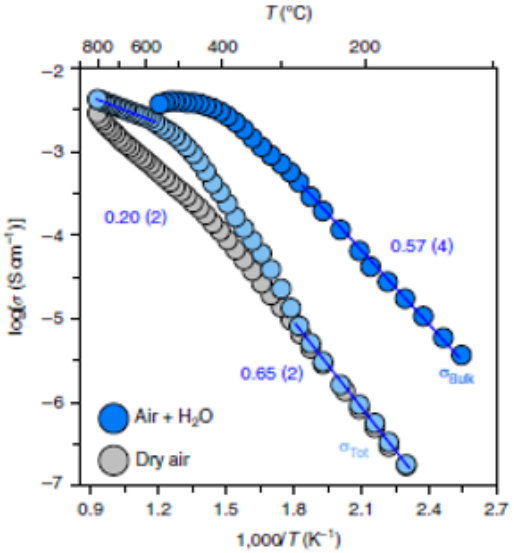

Significant proton transport is only observed above 300 °C

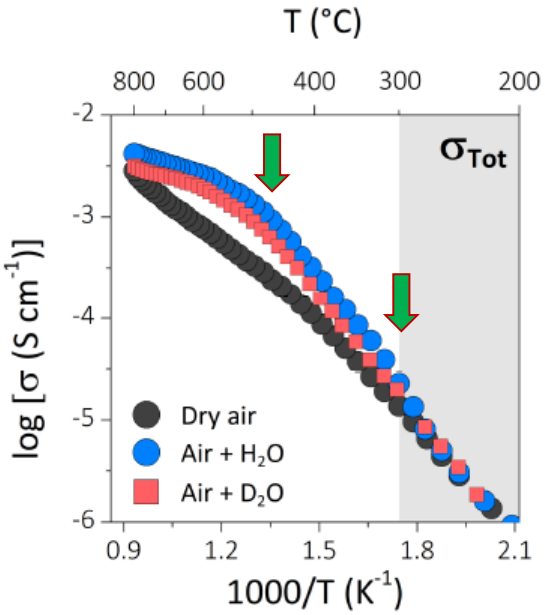

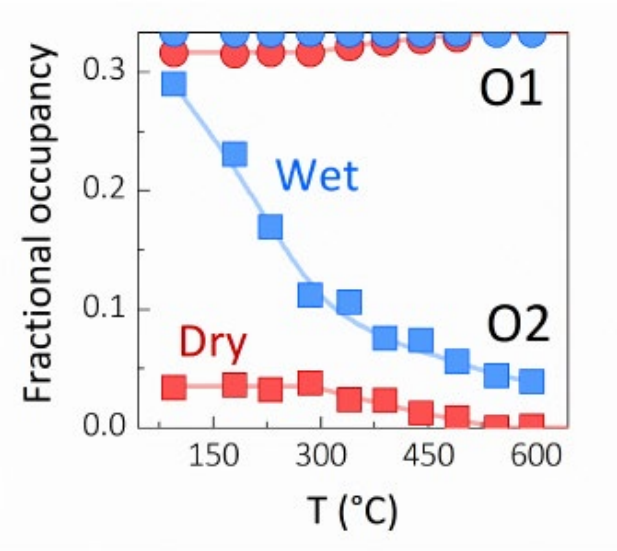

Clear relationship between the structure and the proton conductivity.

The proton conduction appears to be reduced as more water enters at O2.

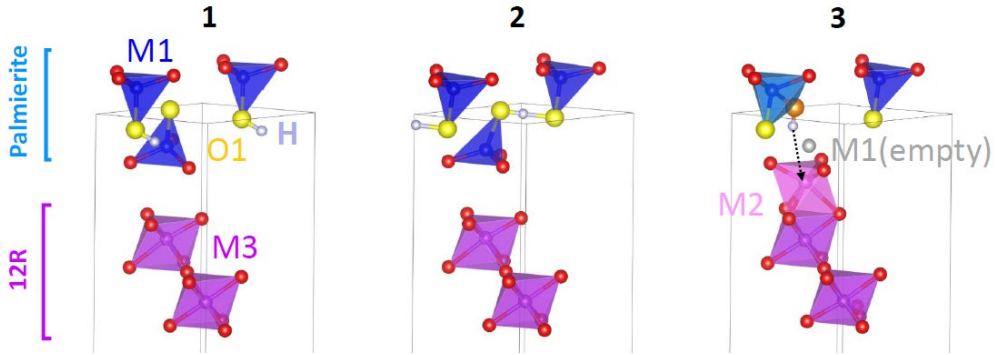

AIMD calculations show that if the proton points directly at a M1 site, it forces movement of the M1 to the M2 site (James Dawson (Newcastle).

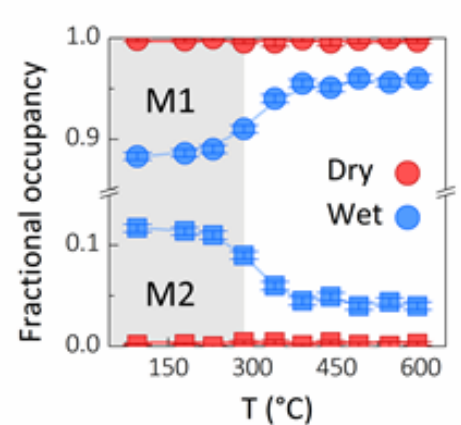

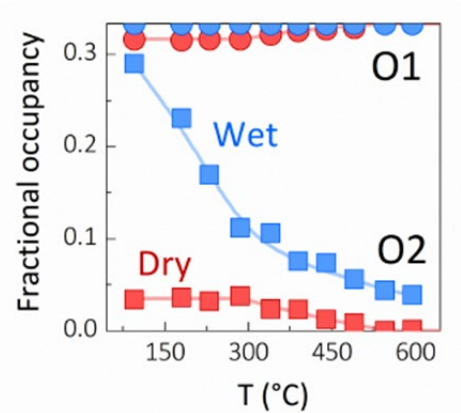

UNIVERSITY OF ABERDEEN

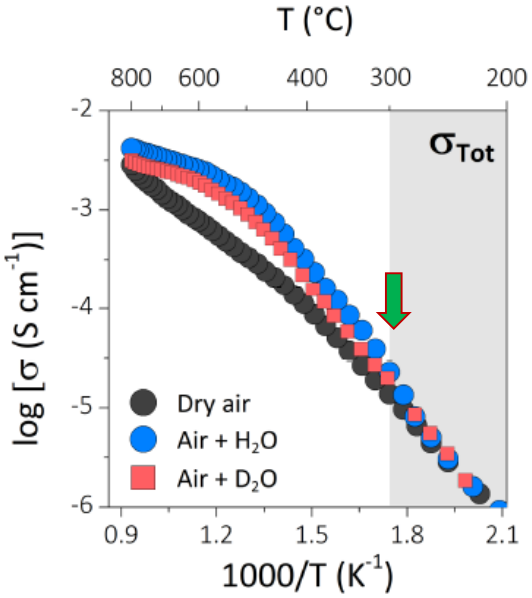

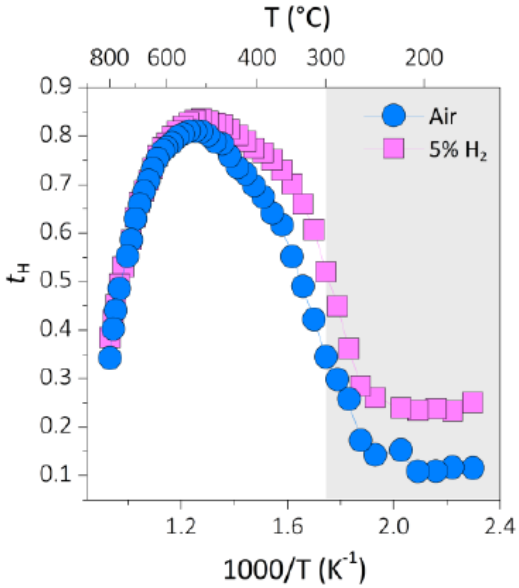

Calculations show strong trapping of the proton at the M1 vacancy.

Results would suggest that trapping of the proton at the M1 vacancy leads to loss of proton conductivity below 300 °C.

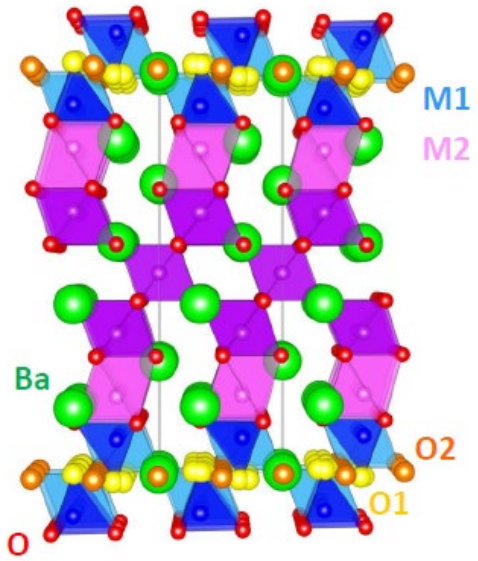

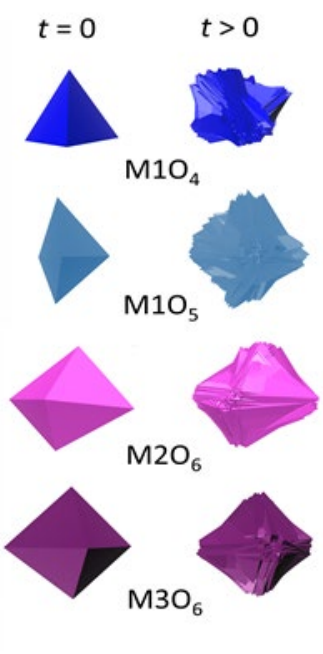

The fast oxide ion and proton migration in $Ba_7Nb_4MoO_{20}$ is enabled by the dynamic and rotational flexibility of the $M1O_x$ units and by the ability of the metal centres of adopting variable coordination environments

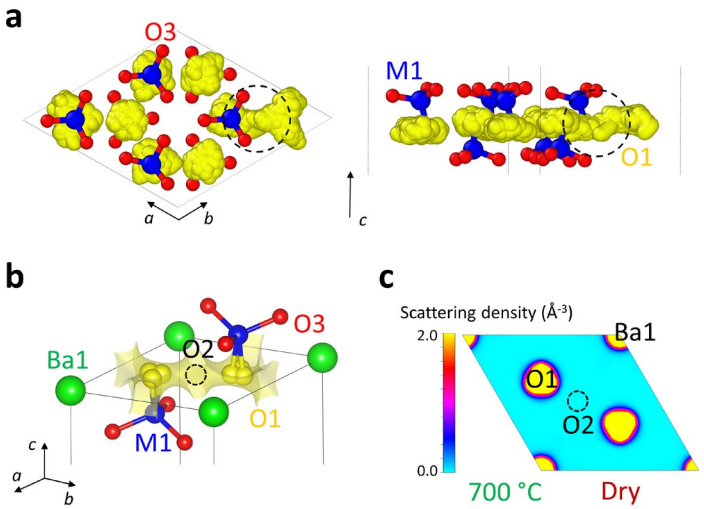

Oxide ion conduction mechanism: At low T continuous scattering density distribution in the palmierite-like layer from MEM and BVSE. Co-operative interstitialcy mechanism.

O2 empty at high T – no continuous scattering between O1 sites. Direct mechanism.

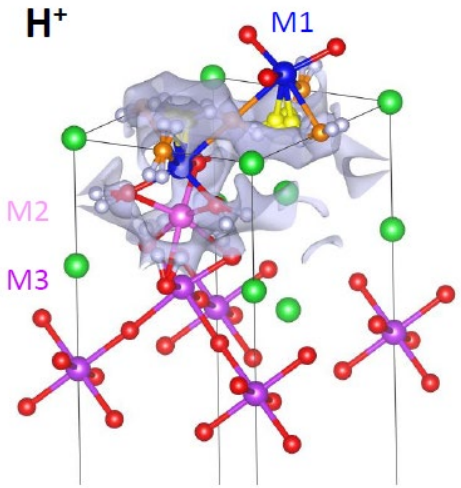

Proton conduction: Complex percolation network around palmierite-like layer.

Frustration of the proton positions (and of the hydrogen bond network) coupled with the dynamic flexibility of the metal units result in high mobility of the protonic defects.

Ionic conducting palmierites – $A_3V_2O_8$
A = Ba, Sr

Ionic conducting palmierites – $A_3V_2O_8$

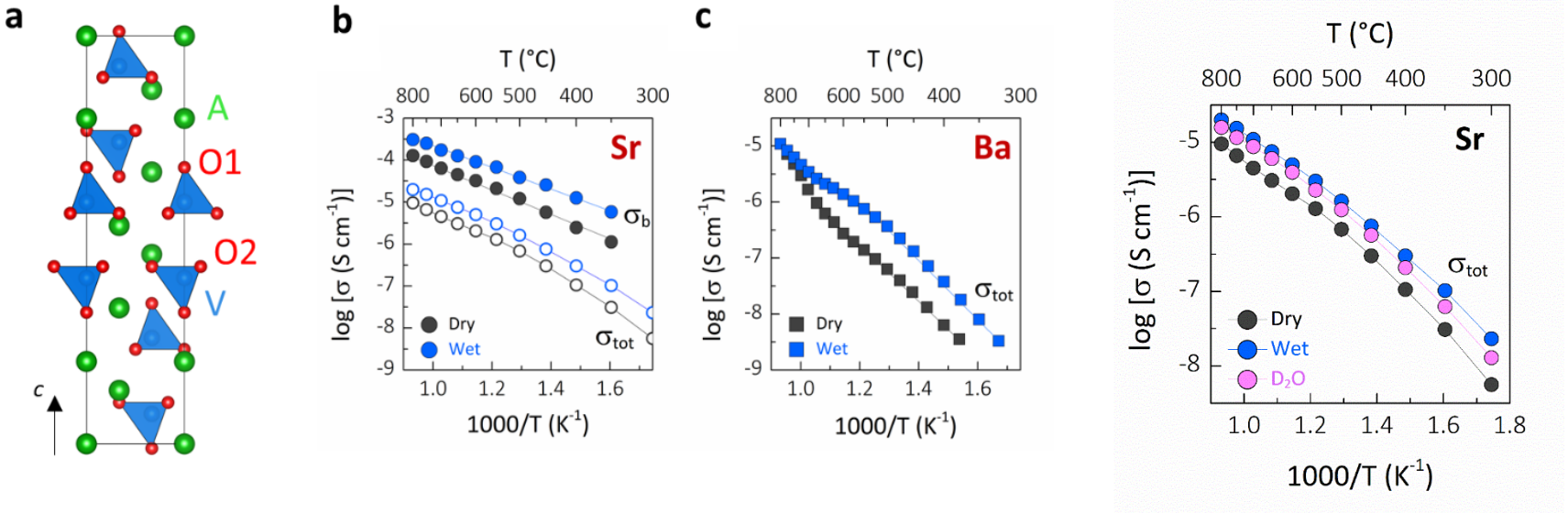

Oxide ion and proton conductivity is observed.

UNIVERSITY OF ABERDEEN

S. Fop *et al*, *Chem. Mater.* 2022 (in press)

Ionic conducting palmierites – $A_3V_2O_8$

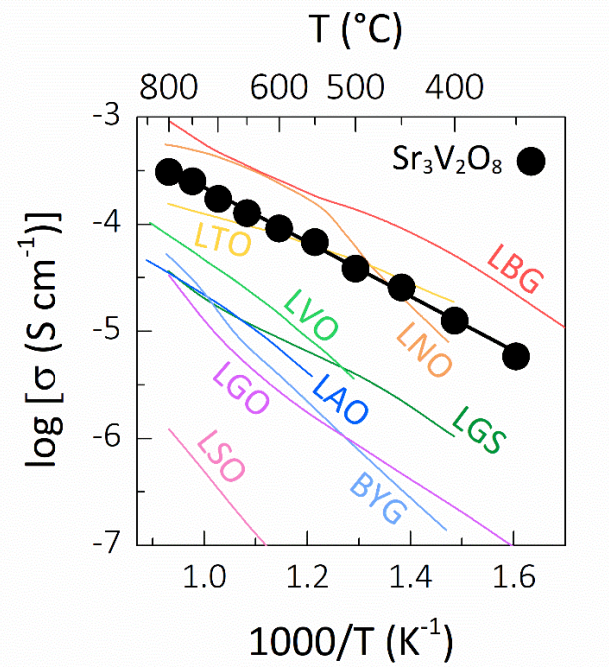

Currently undoped

High conductivity compared to other doped phases containing isolated tetrahedra

Bond-valence site energy calculations using *soft*BV.
Map out migration pathway and energy landscape.

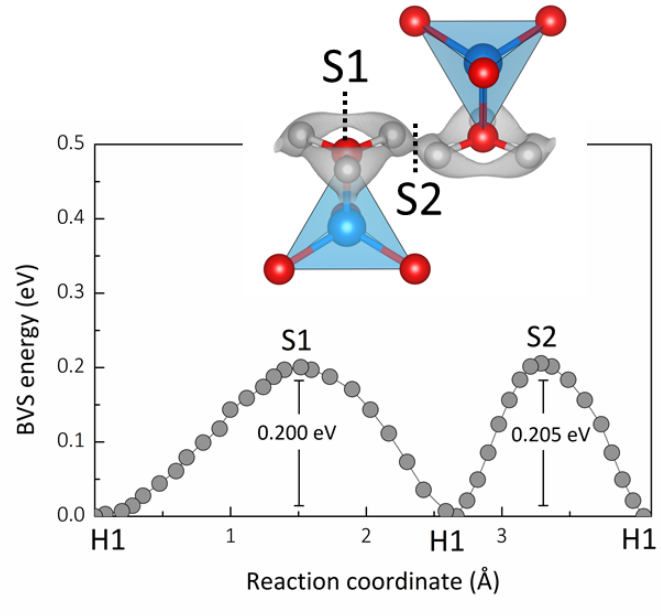

Low energy 2D conduction pathway for protons

S1 = exchange

S2 = hopping

UNIVERSITY OF ABERDEEN

AIMD simulations show oxide ion conductivity is only possible if there are a small amount of intrinsic oxide ion vacancies.

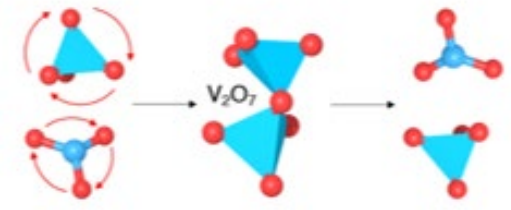

Oxide ion transport occurs via the formation of V_2O_7 groups.

Rotation of VO_4 groups is pivotal in facilitating ion transport

Intrinsic oxide ion vacancies also enable absorption of water into the structure.

Targeted chemical doping to enhance the conductivity.

Summary

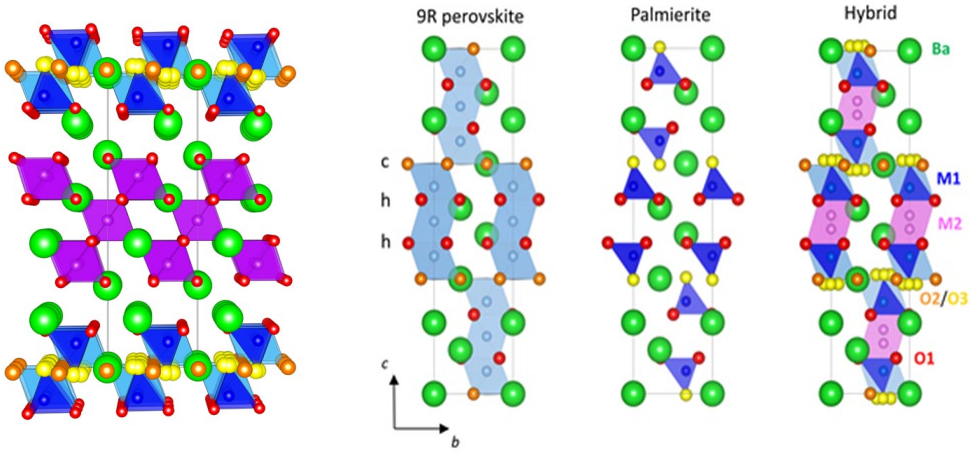

We've now investigated several different hexagonal perovskite derivatives which show fascinating electrical and structural properties.

Further study of hexagonal perovskite derivatives containing mixed tetrahedral and octahedral geometry could open up a new direction in the design of novel oxygen (and proton) conducting electrolytes.

Acknowledgements

- Sacha Fop, Kirstie McCombie, Asma Gilane, Dylan Tawse, Sophie Martin, Victoria Watson, Yi Sun.
- Jan Skakle, Eve Wildman,

  John Irvine, Paul Connor, Cristian Savaniu, James Dawson
- Clemens Ritter, Ron Smith, Dominic Fortes
- EPSRC MISE
- Leverhulme trust

UNIVERSITY OF ABERDEEN

EPSRC Engineering and Physical Sciences Research Council

MISE

LEVERHULME TRUST

Wet Conditions

Proton location

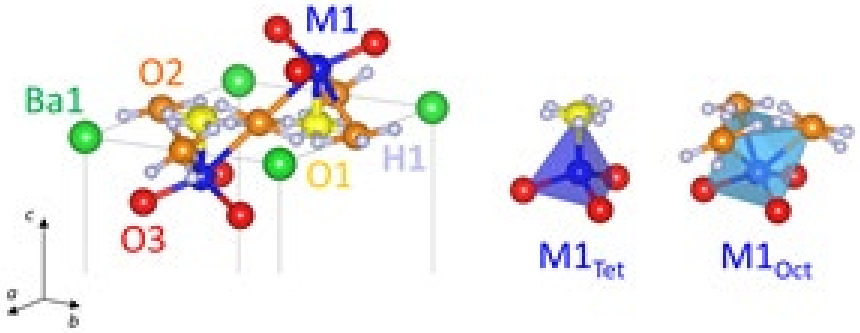

The deuteron atom is located in proximity of the average O1 and O2 sites, on six equivalent positions.

D2B, ILL at 4 K.

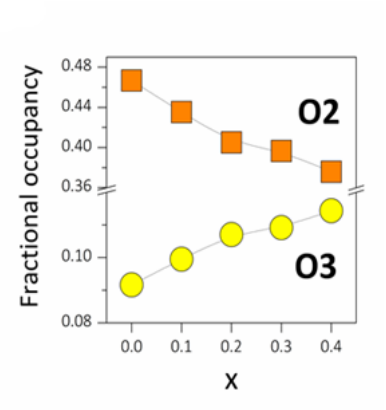

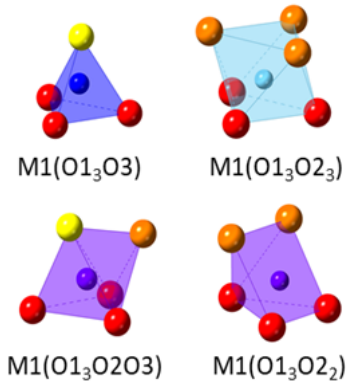

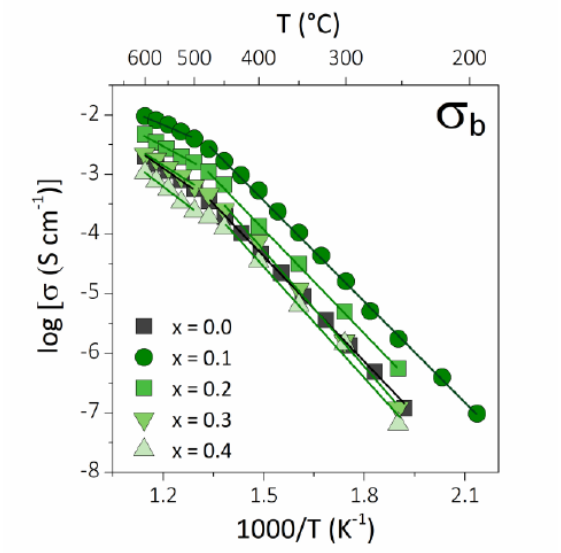

Results show V substitution results in an increase of the number of tetrahedra in the palmierite layer.

The highest conductivity is observed for x = 0.1. Why?

UNIVERSITY OF ABERDEEN

S. Fop et al, *Chem. Mater.*, 2020, 32, 4724.

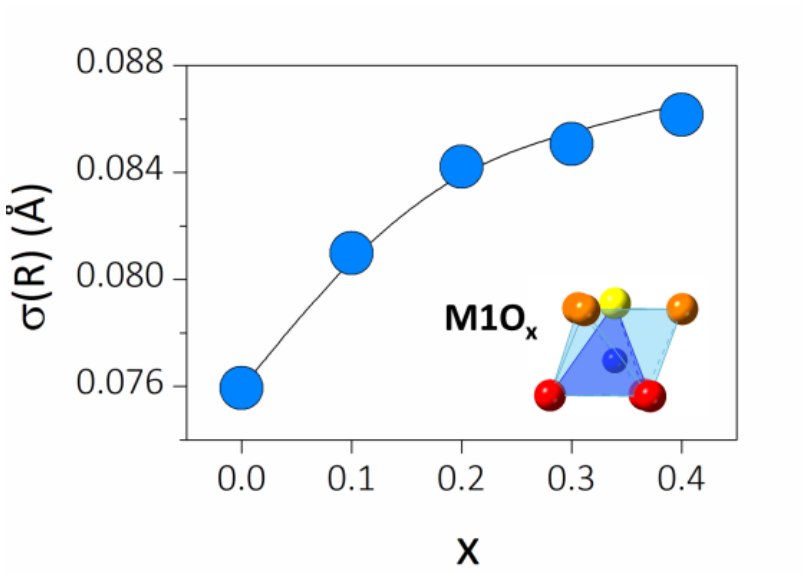

The polyhedra become more distorted upon increasing x.

Can act as a trap for mobile defects.

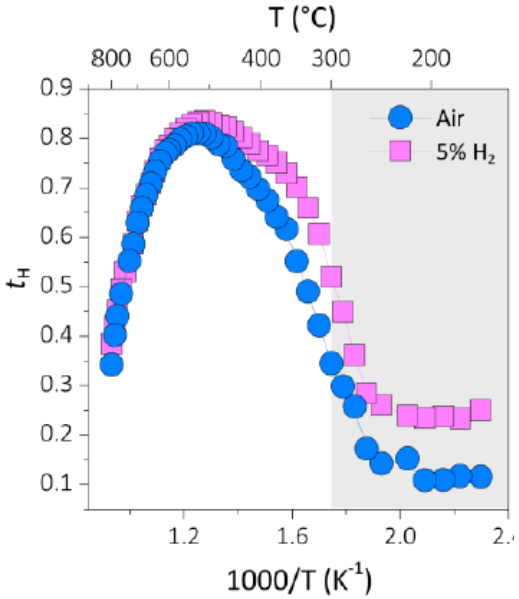

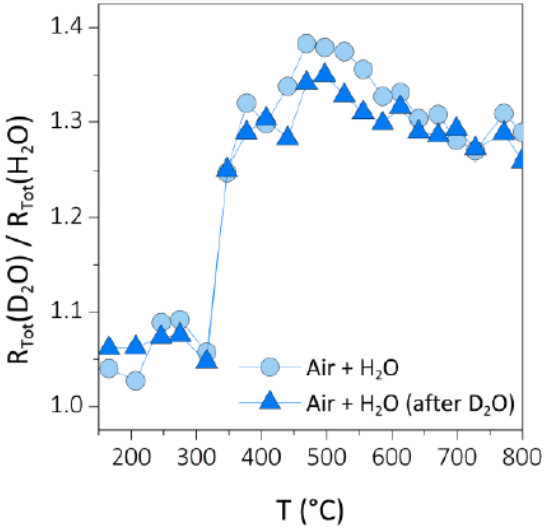

Significant proton transport is only observed above 300 °C

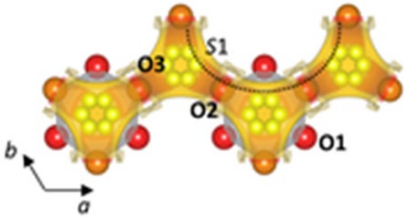

S1: oxide ion exchange along the connected distribution of average oxygen sites O2/O3.
E1 decreases with V doping.

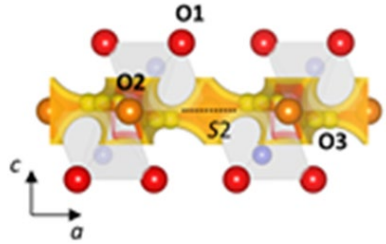

S2: is perpendicular to the undulating distribution of crystallographic oxygen sites.

Migration along the *ab* plane requires a relaxation of the oxygen atoms in direction parallel to the *c*-axis of ~ 0.25 Å as a result of the undulating distribution of crystallographic sites.
E2 increases with V doping.

*E*2 is associated with the relaxation of the metal polyhedra during the oxygen exchange and therefore its height will be linked to the average distortion of the $M1O_x$ units.

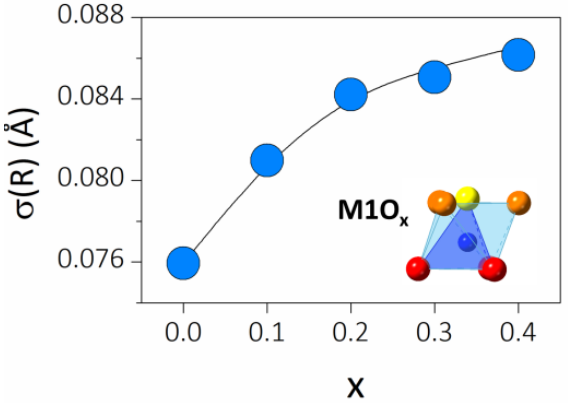

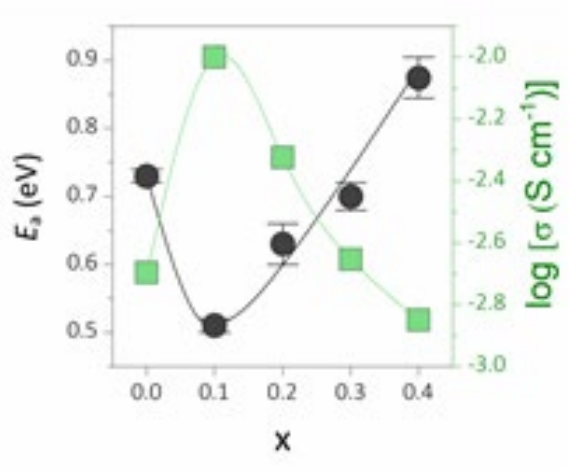

The structure becomes more distorted upon increasing x, enhancing E2.

Can act as a trap for mobile defects.

Competing energy barriers results in optimum conductivity for x = 0.1.

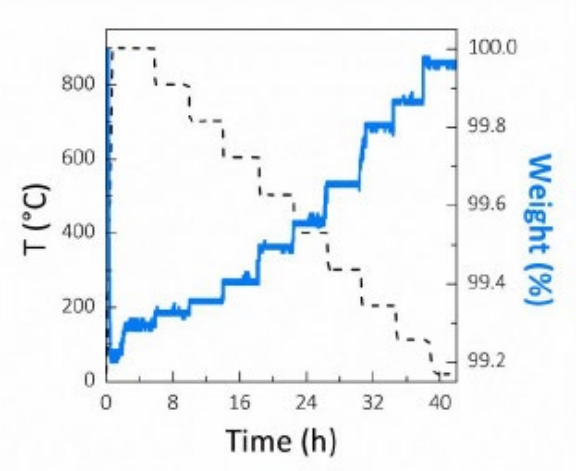

Uniform water uptake

$Ba_7Nb_4MoO_{20} \cdot 0.8H_2O$

Dissociative absorption of water

$$H_2O_{(g)} + V_O^{\bullet\bullet} + O_O^X \leftrightarrow 2OH_O^{\bullet}$$

More favorable above 300 °C

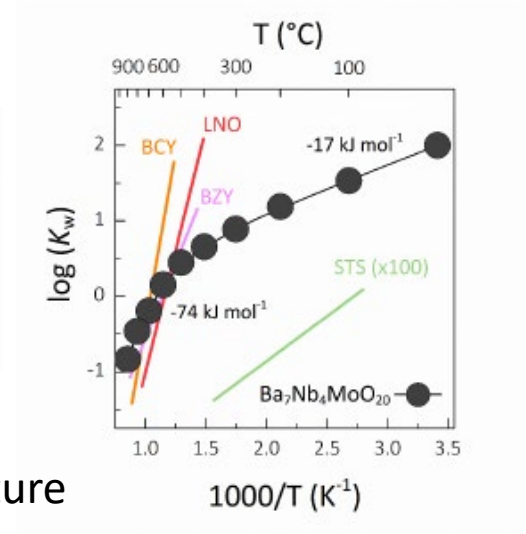

Suggests change in crystal structure

1495 UNIVERSITY OF ABERDEEN

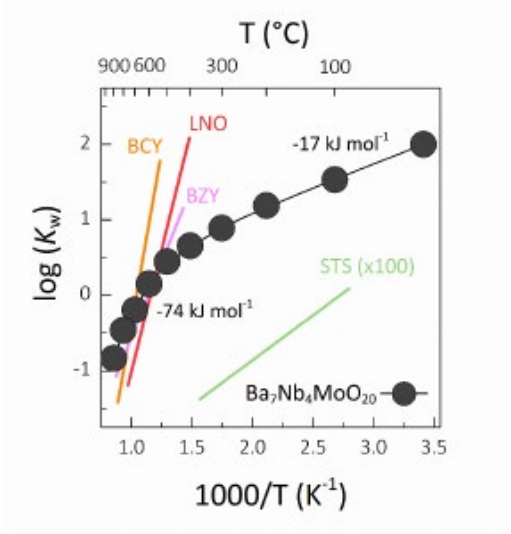

$\Delta H^0 = -18$ kJ mol^{-1}
and $\Delta S^0 = -31$ J K^{-1} mol^{-1}; at higher temperatures, $\Delta H^0 = -74$ kJ mol^{-1} and $\Delta S^0 = -101$ J K^{-1} mol^{-1}.

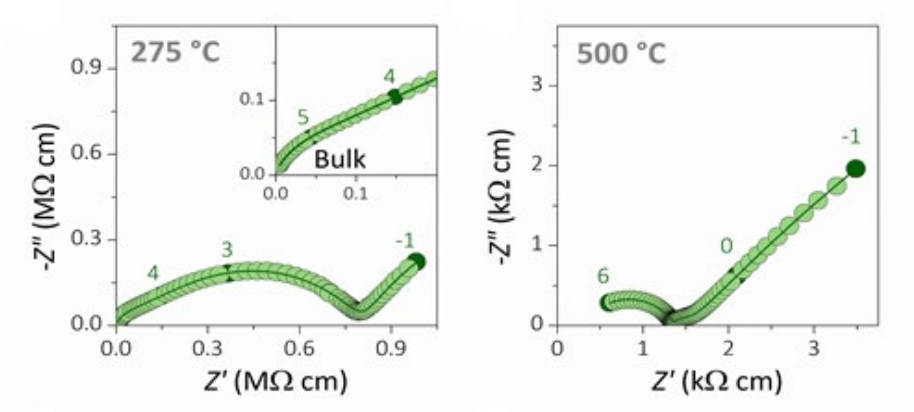

Impedance spectroscopy takes into account both the resistive and reactive components and discerns the electrical responses of the different regions of the system according to their time constants.

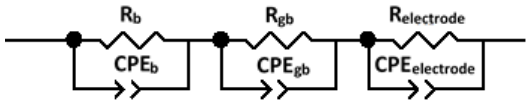

UNIVERSITY OF ABERDEEN

Electrical Measurements – dry air

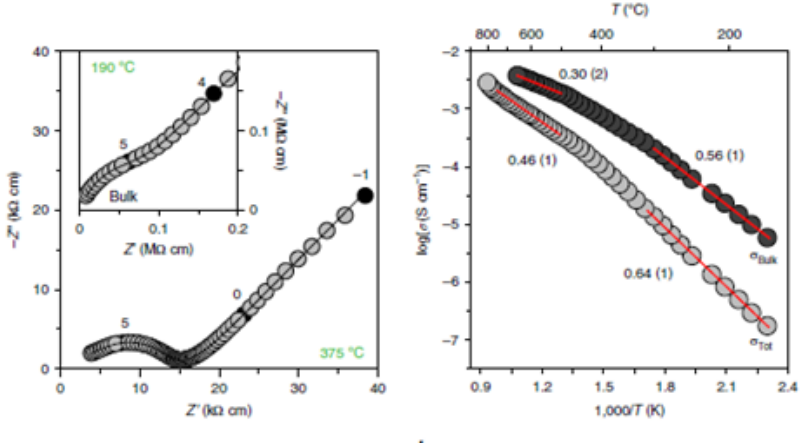

Impedance spectroscopy takes into account both the resistive and reactive components and discerns the electrical responses of the different regions of the system according to their time constants.

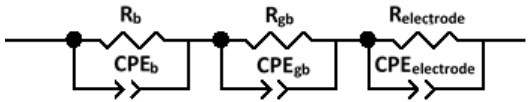

1495 UNIVERSITY OF ABERDEEN

Electrical Measurements – wet air

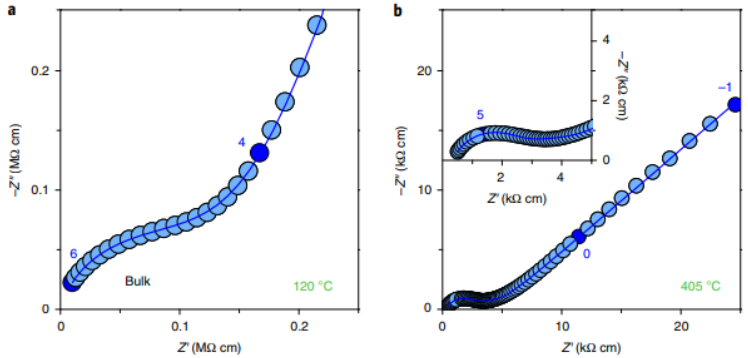

Impedance spectroscopy takes into account both the resistive and reactive components and discerns the electrical responses of the different regions of the system according to their time constants.

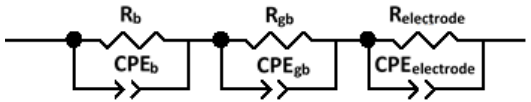

1495 UNIVERSITY OF ABERDEEN

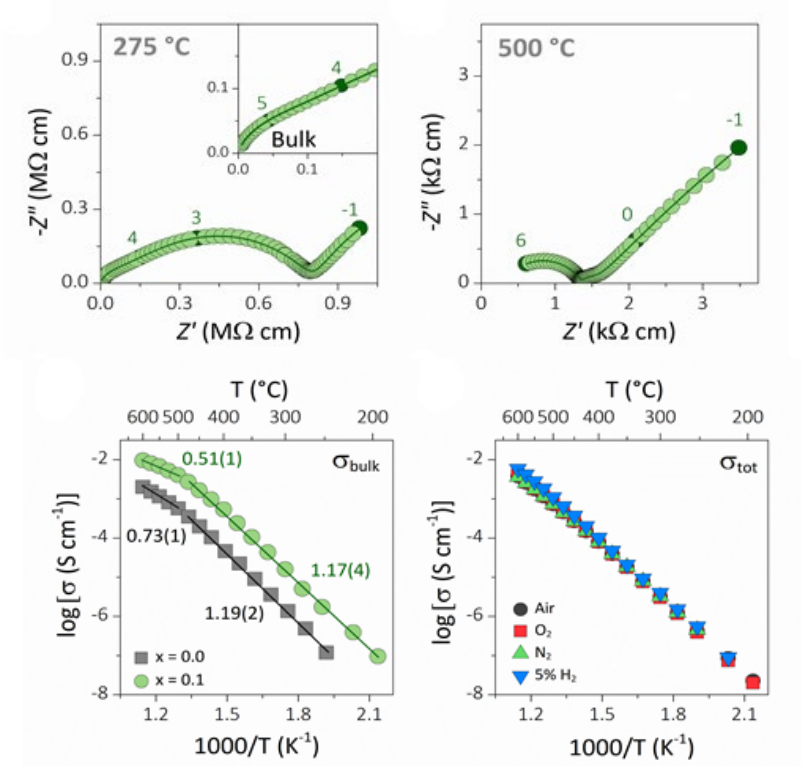

The bulk conductivity of $Ba_3Nb_{0.9}V_{0.1}MoO_{8.5}$ is almost an order of magnitude higher than that of $Ba_3NbMoO_{8.5}$.

Electrical characterisation

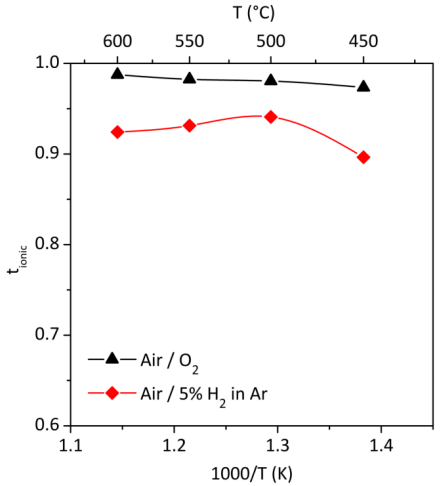

Concentration cell measurements

$$t_{ionic} = \frac{\sigma_{ionic}}{\sigma_{tot}} = \frac{E_{obs}}{E_{Nernst}}$$

Results suggest $Ba_3NbMoO_{8.5}$ is an oxide ion conductor with negligible electronic conductivity in air/O_2.

A small amount of electronic conduction is observed in air/5% H_2 in Ar

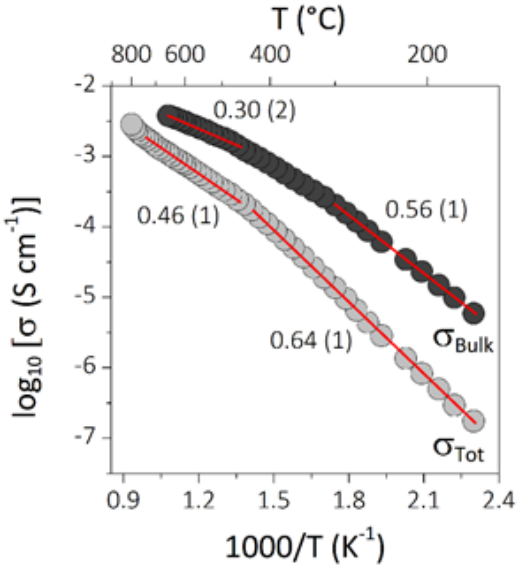

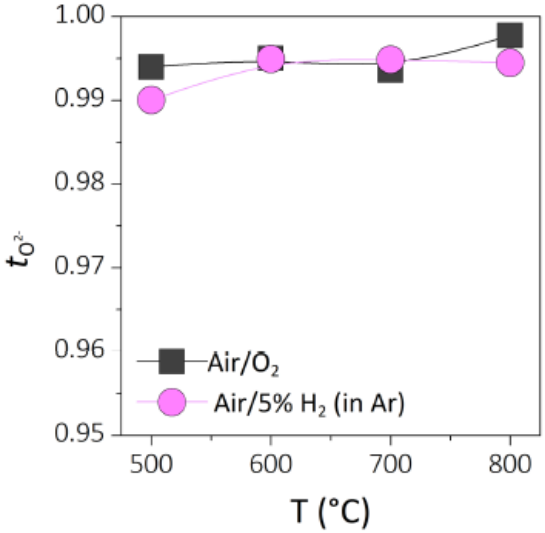

Transport measurements show negligible electronic conductivity in air/O_2 or air/5% H_2 in Ar.

UNIVERSITY OF ABERDEEN

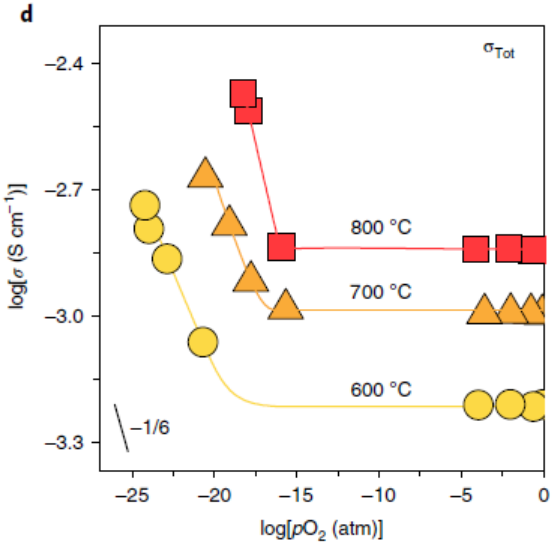

pO_2 measurements show the electrolytic domain of $Ba_7Nb_4MoO_{20}$ extends between ~10^{-18}–1 atm at 600 °C,

Structural Model

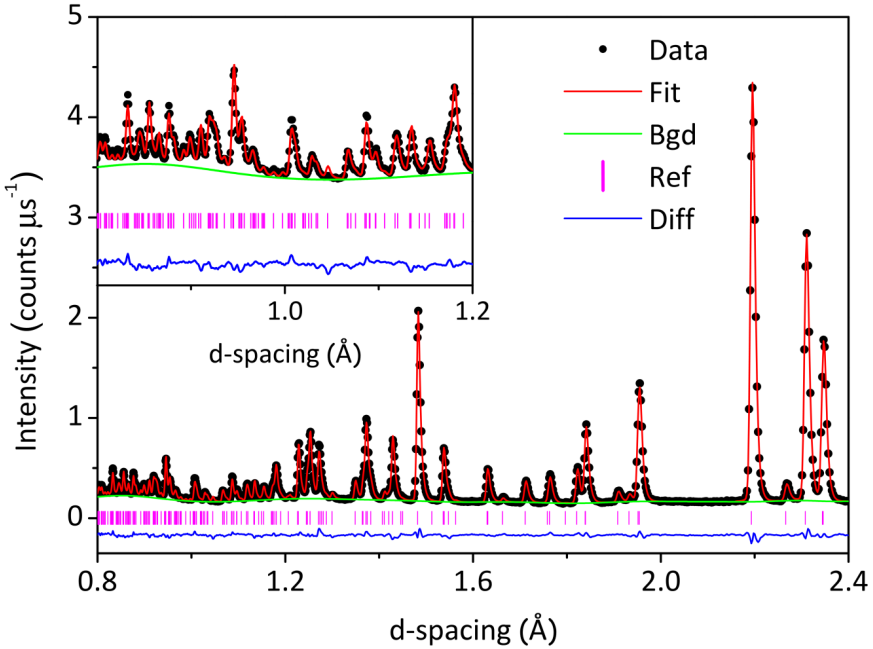

$\chi^2 = 2.4$

$R_p = 3.29\%$

$R_{wp} = 3.24\%$

Space group $R\bar{3}m$ H, $a = b = 5.92744\ (3)$ Å, $c = 21.0995\ (2)$ Å, V = 642.002 (6) Å^3

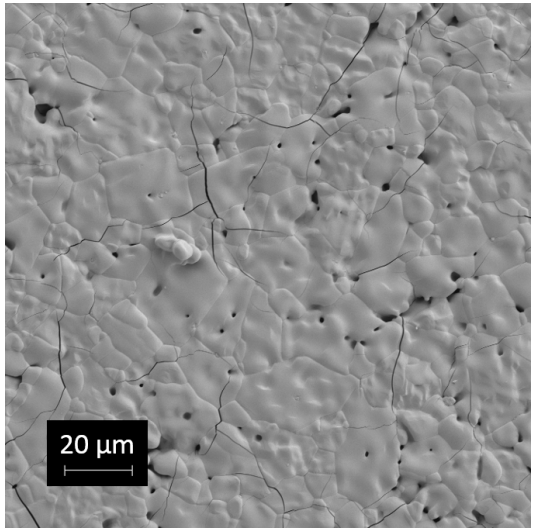

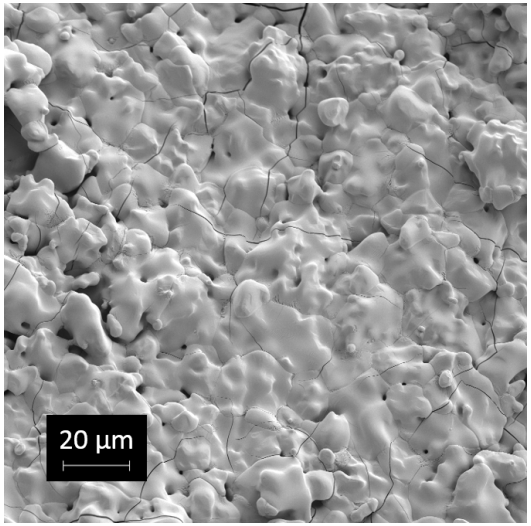

SEM $Ba_3WNbO_{8.5}$

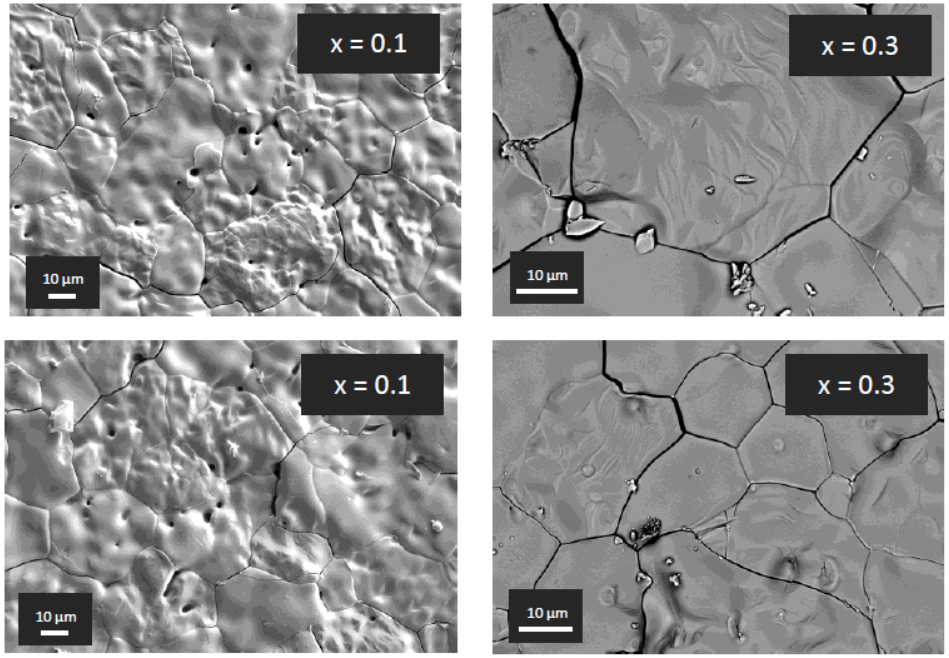

SEM $Ba_3MoNb_{1-x}V_xO_{8.5}$

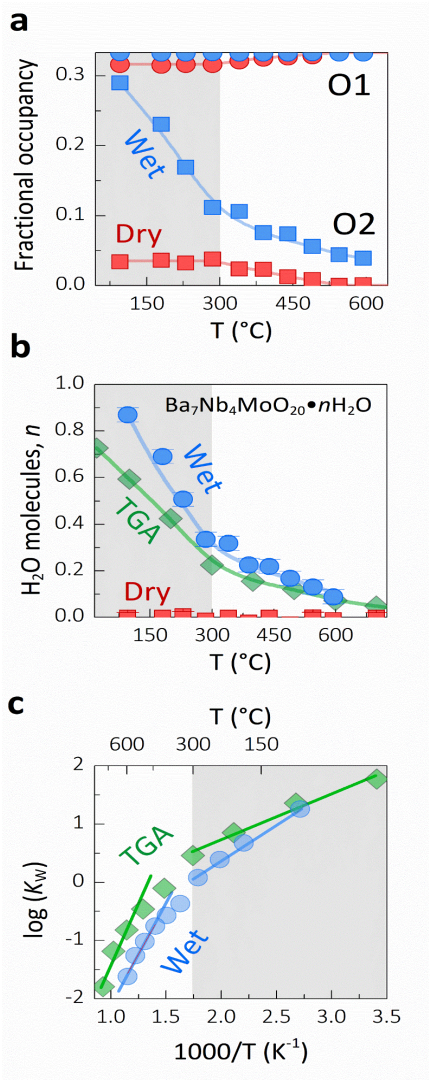

UNIVERSITY OF ABERDEEN

The local structure was determined by total scattering experiments and pair distribution function analysis.

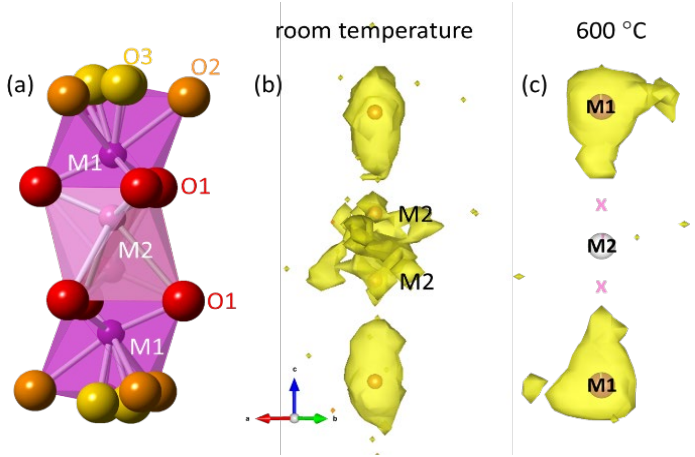

Atomic density map of M1 and M2 sites. Metals are disordered. At 600 °C only the M1 site is significantly populated.

At room temperature 5-fold co-ordination is prevalent (45%). Upon heating to 600 °C there is an increase in the number of tetrahedra and decrease in the number of octahedra as seen in the average structure.

M. S. Chambers *et al J. Mat. Chem. A* (submitted).

Oxide ion conduction pathway – atomic density cross section of O(2) and O(3) viewed down *c*.

Room temperature 600 °C

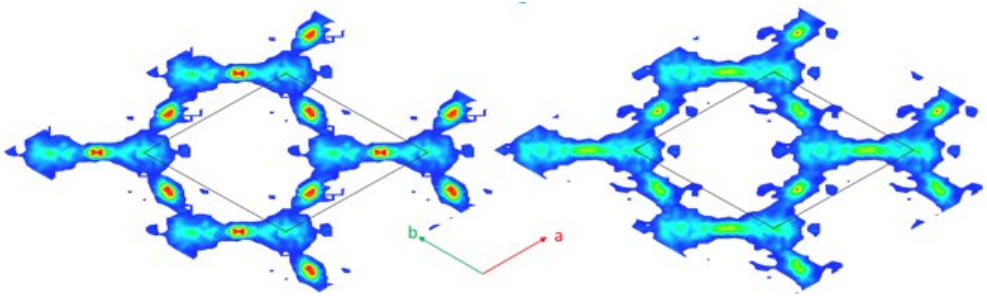

At 600 °C there is an almost continuous distribution of oxygen atoms around the hexagonal rings of the structure.

Easy diffusion of the oxide ions in two dimensions.

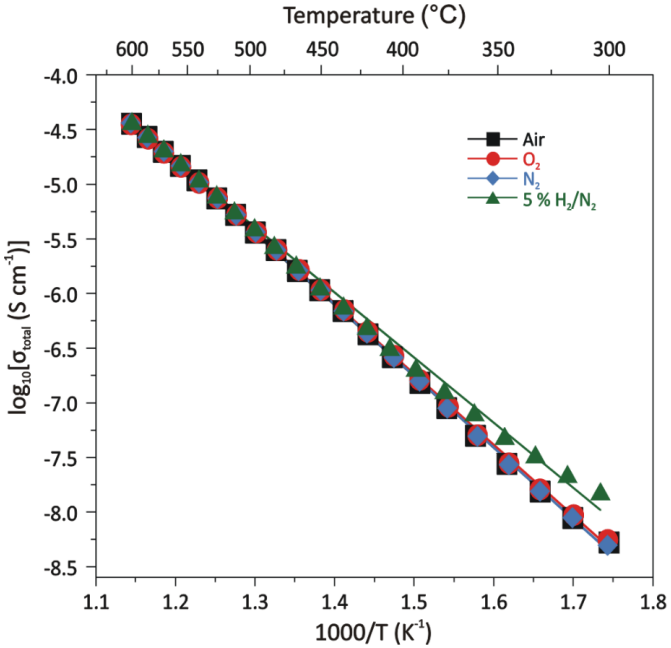

$Ba_3W_{1.2}Nb_{0.8}O_{8.6}$ also exhibits negligible electronic conductivity in reducing atmospheres!

$$nOct = \{[O(2)\_Occ \times 9]/1.5\} \times M(1)\_Occ\}$$

$$nTet = \{[O(3)\_Occ \times 18]/1\} \times M(1)\_Occ\}$$